IR and UV Imaging @ SOLEIL Synchrotron

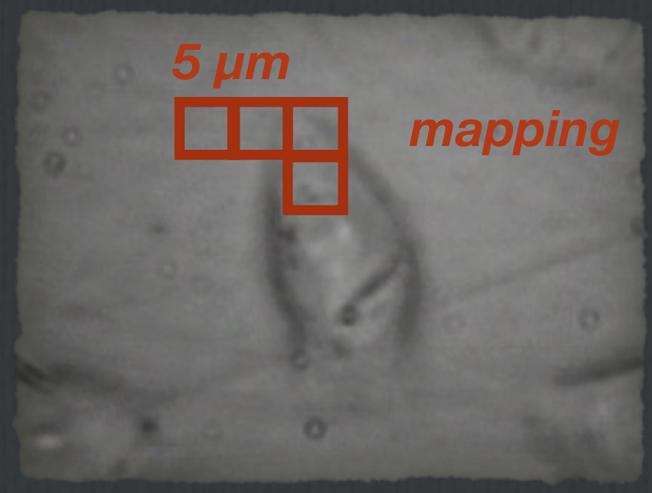


- Infrared Imaging : SMIS beamline
- DUV Imaging : DISCO Beamline

frederic.jamme@synchrotron-soleil.fr

☐ smis beamline





Since the early 90s and more specifically during the last decade, infrared microspectroscopy at synchrotron facilities has been largely exploited. The main reasons of the utilisation of that electromagnetic radiation are enhanced lateral resolution (typically at or very close to the diffraction limit), superior signal to noise obtained without resorting to prohibitively long acquisition times, and wide energy range availability. At the SOLEIL synchrotron, the SMIS beamline (Spectroscopy and Microscopy in Infrared using Synchrotron) is operational since January 2008, and several important studies have been achieved on single cells and tissues.

Dumas, P., Polack, F., Lagarde, B., Chubar, O., Giorgetta, J., and Lefrancois, S. Synchrotron infrared microscopy at the French Synchrotron Facility SOLEIL, 2006, Infrared Physics & Technology 49, 152–160.

SMIS
IR 8000-350 cm^{-1}



IR Microscopes:

- Continuum XL (dedicated to biology)
- Continuum
- NicPlan
- Home made IR microscope (high pressure)

- In10 (for imaging)

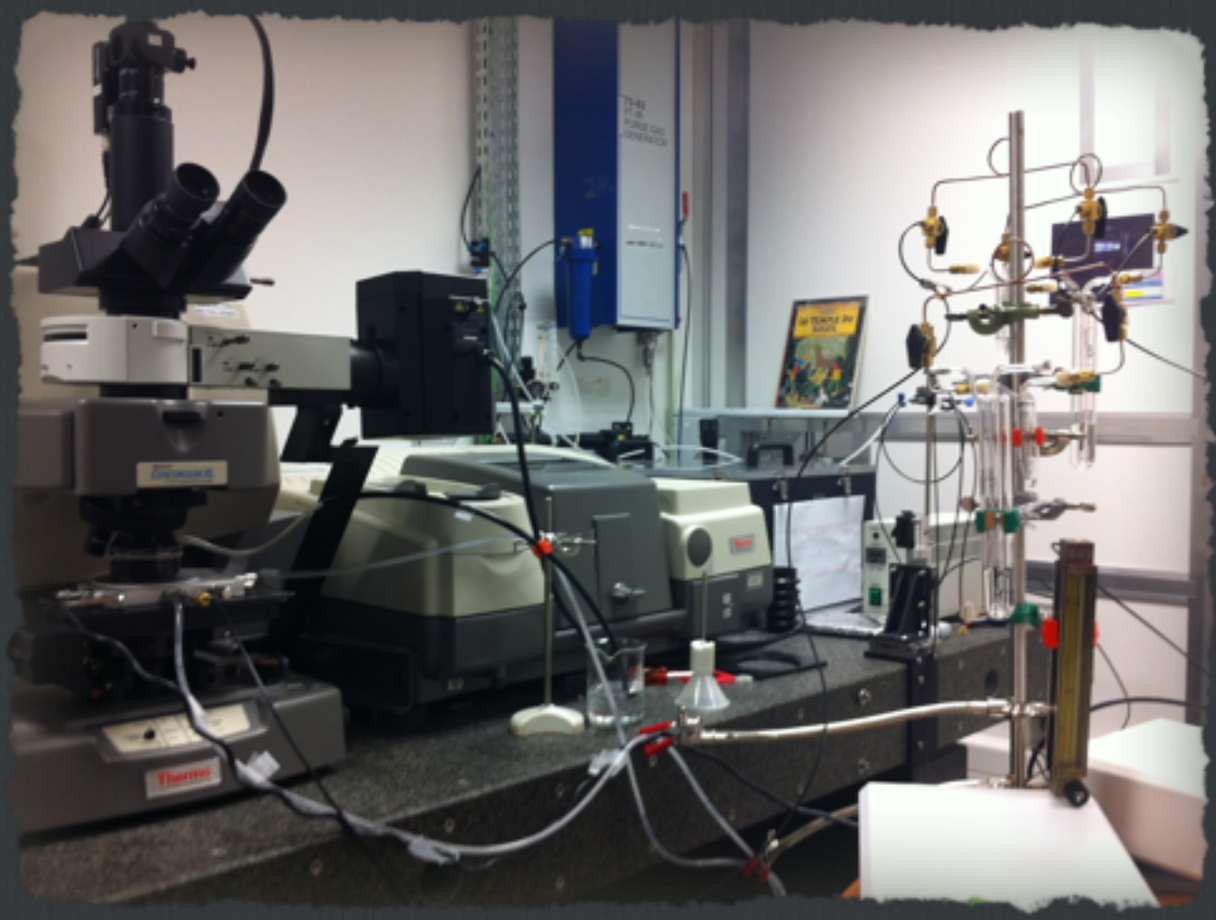
Raman Microscope:

DXR (Thermo Fischer)

Sample environment:

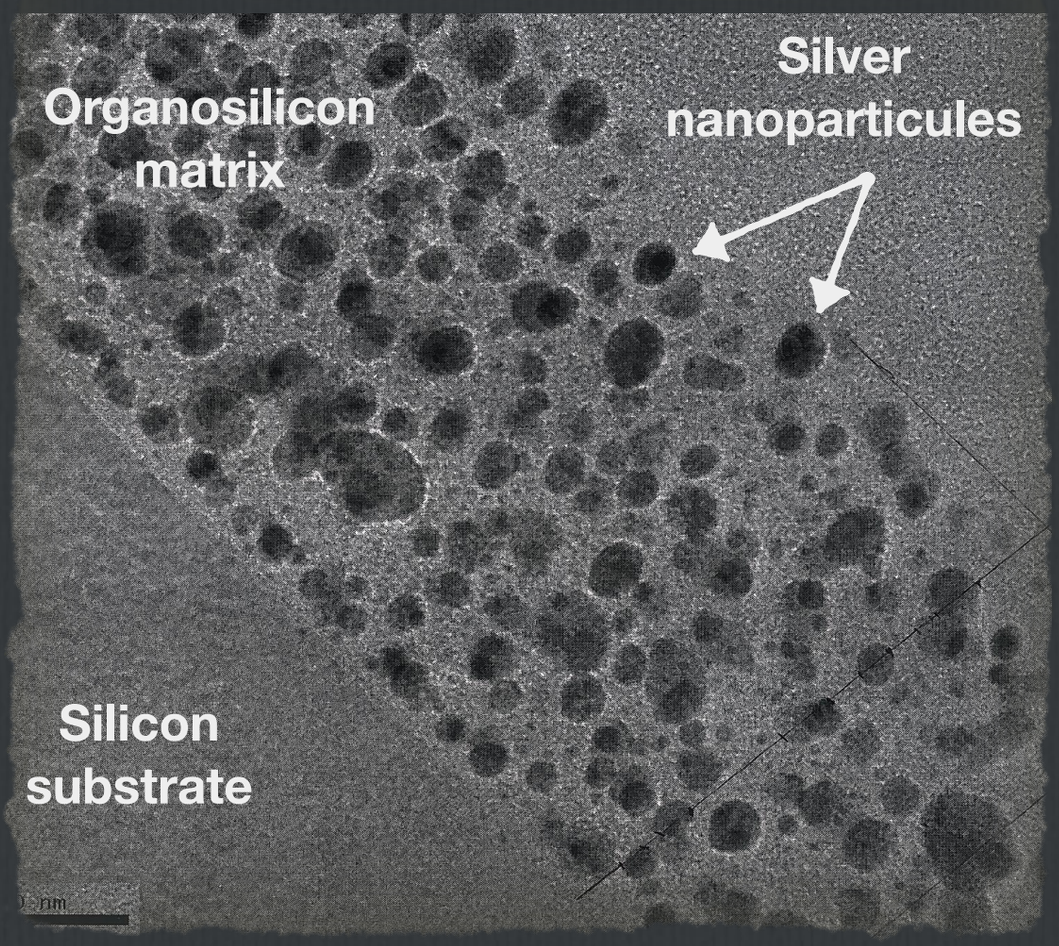
Heating stage
Vacuum Stage
Stretching stage
Pressure (anvil diamond)

SMIS Highlights



Synchrotron FTIR microspectroscopy of the yeast Saccharomyces cerevisiae after exposure to plasma-deposited nanosilver-containing coating

C. Saulou, F. Jamme, C. Maranges, B. Despax, P. Raynaud, P. Dumas and M. Mercier-Bonin

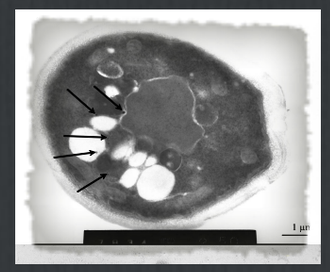


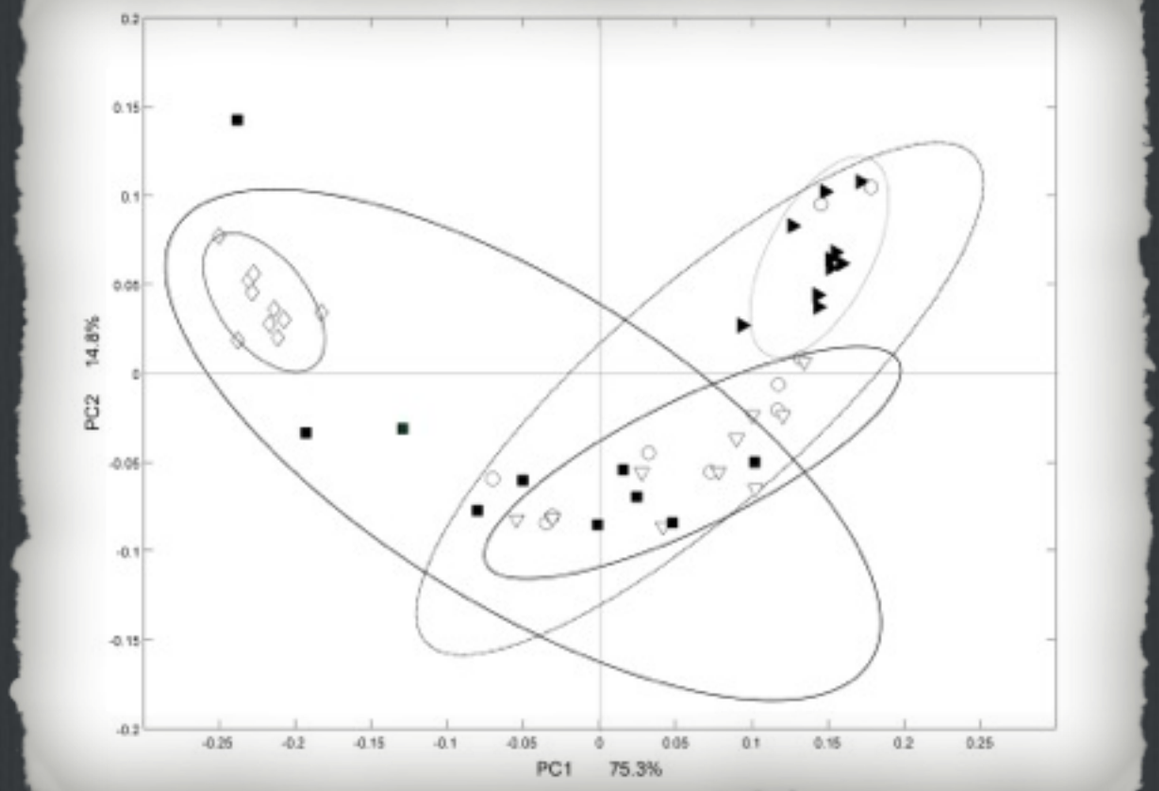
The present work was focused on elucidating changes in the model yeast Saccharomyces cerevisiae (cell composition, ultrastructure) after exposure to antimicrobial plasma-mediated nanocomposite films. In addition, scanning electron microscopy (SEM) demonstrated the nanoparticle-based morphology of the deposited layer. The antifungal properties towards S. cerevisiae were established, since a 1.4 log reduction in viable counts was observed after a 24-h adhesion compared to control conditions with the matrix alone.

Differences in cell composition after exposure to the nanosilver was assessed for the protein region using, synchrotron Fourier-transform infrared (FTIR) microspectroscopy of single S. cerevisiae cells, through in situ mapping with sub-cellular spatial resolution.

Anal Bioanal Chem 2009, vol. 396, pp. 1441–1450

Synchrotron FTIR microspectroscopy of the yeast Saccharomyces cerevisiae after exposure to plasma-deposited nanosilver-containing coating





In situ **mapping with high spatial resolution (5 x 5 µm² aperture)**

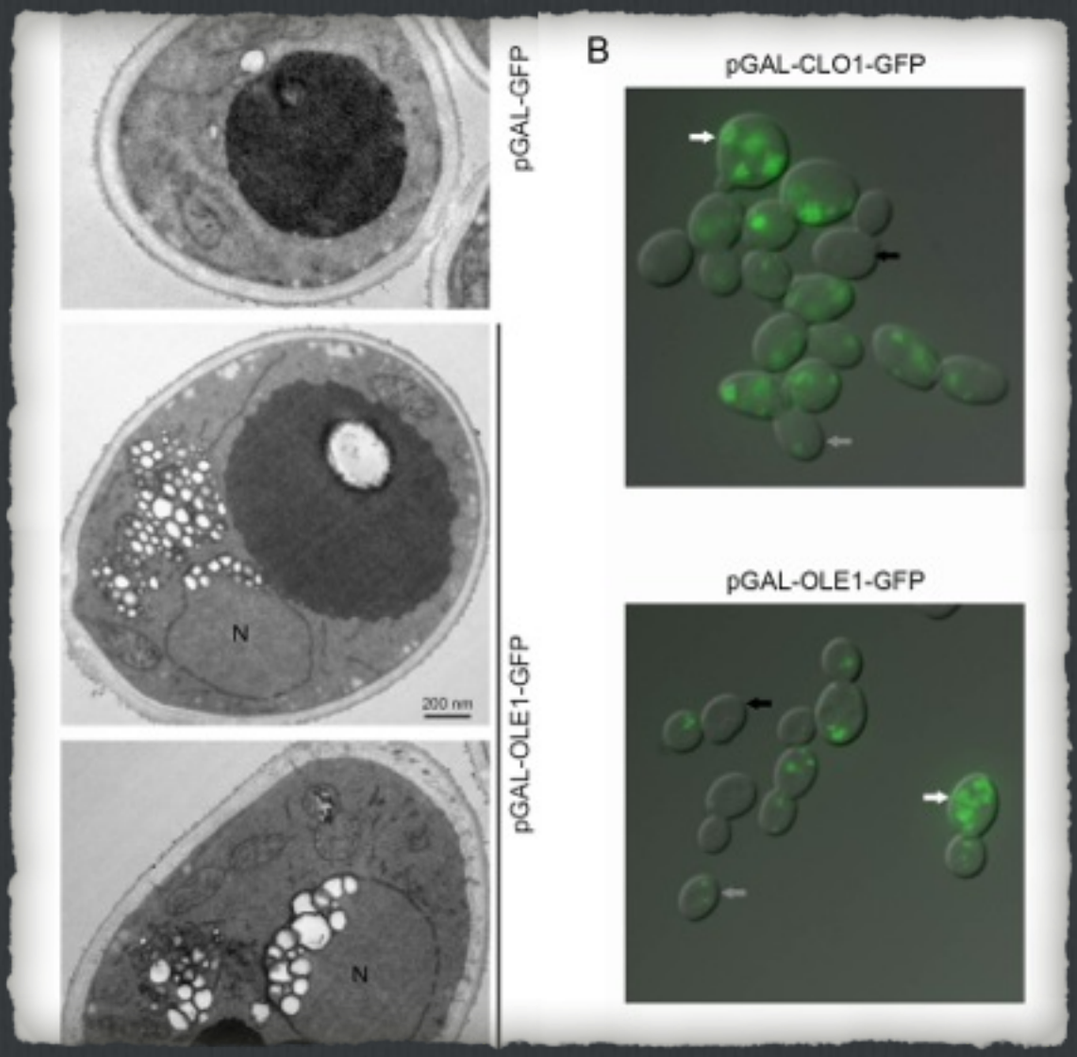
IR spectrum of yeast cells recovered after a 24-h adhesion to the nanosilver-containing coating revealed a significant downshift (20 cm(-1)) of the amide I peak at 1655 cm(-1), compared to freshly harvested cells. This lower band position, corresponding to a loss in alpha-helix structures, is indicative of the disordered secondary structures of proteins, due to the transition between active and inactive conformations under nanosilver-induced stress conditions.

The inhibitory action of silver was targeted against both cell wall and intracellular proteins such as enzymes. Transmission electron microscopy (TEM) observations of the yeast ultrastructure confirmed serious morphological and structural damages. A homogeneous protein-binding distribution of nanosilver all over the cell was assumed, since the presence of electron-dense silver clusters was detected not only on the cell surface but also within the cell. For control experiments with the organosilicon matrix alone, no antimicrobial effect was observed, which was consistent with synchrotron FTIR results and TEM observations.

Anal Bioanal Chem 2009, vol. 396, pp. 1441–1450

Single Cell Synchrotron FT-IR Microspectroscopy Reveals a Link between Neutral Lipid and Storage Carbohydrate Fluxes in S. cerevisiae

Frederic Jamme, Jean-David Vindigni, Valérie Méchin, Tamazight Cherifi, Thierry Chardot, and Marine Froissard

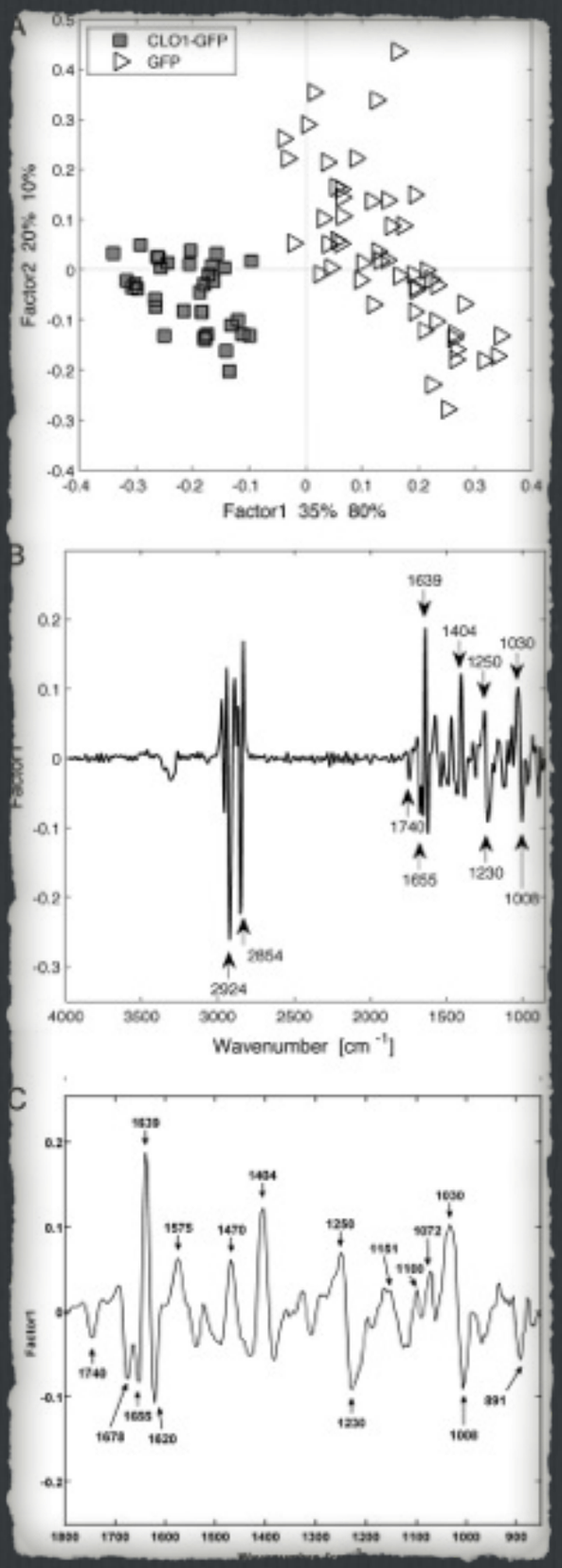


The phenotype of these cells was explored using synchrotron FT-IR microspectroscopy to investigate the dynamics of lipid storage and cellular carbon fluxes reflected as changes in spectral fingerprints.

Multivariate statistical analysis of the data showed a clear effect on storage carbohydrates and more specifically, a decrease in glycogen in our modified strains.

These observations were confirmed by biochemical quantification of the storage carbohydrates glycogen and trehalose. Our results demonstrate that neutral lipid and storage carbohydrate fluxes are tightly connected and co-regulated.

PLoS ONE 2013 vol. 8 (9), p. e74421



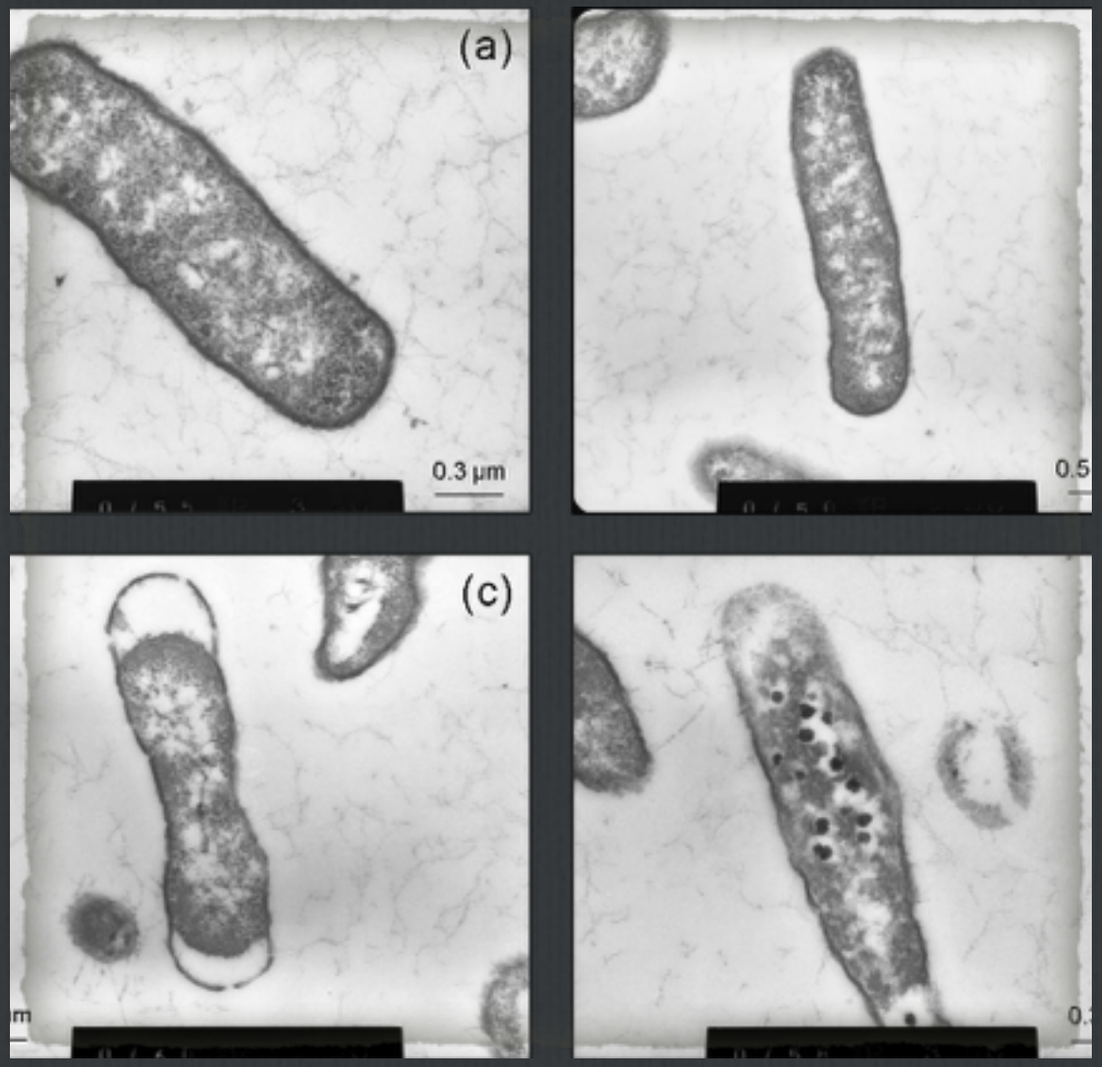
The set of data collected for the GFP expressing **control cells** after 42 h and for **AtClo1-GFP expressing cells**, as these had the **higher fatty acid and neutral lipid content as revealed in the chromatography experiments.** PLS analysis on the full spectral range of these two populations showed a **correlation** between **lipid** specific absorption band variations (Figure below) and additional band variations. In particular, we found a direct correlation between lipid accumulation and the 1008 cm^{-1} band attributed to C=C, potentially due to an increased **unsaturated fatty** acid content. We detected some shifts in the regions corresponding to **Amide stretching** bands suggesting some **protein structure modifications.** We also noticed an **inverse correlation** between some of the lipid bands and the region between 1020 and 1150 cm^{-1} assigned to carbohydrate stretching and more specifically to **glycogen** vibrations (1151, 1100, 1072 and 1030 cm^{-1}).

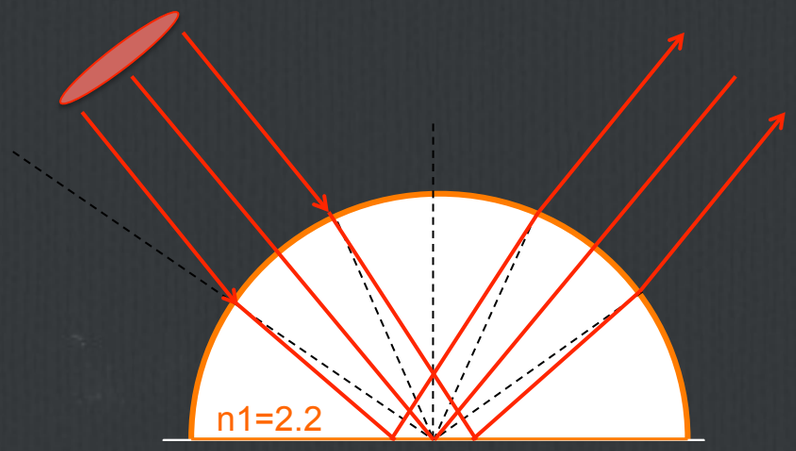
Figure. Multivariate statistical analysis (PLS) of spectra obtained for GFP and AtClo1-GFP expressing cells after 42 h of galactose induction. Score plot (A) of the factor 1 and factor 2 axes and the corresponding loading plot of the factor 1 axis (total range in (B) and zoom between 850 and 1800 cm^{-1} in (C)) are presented.

PLoS ONE 2013 vol. 8 (9), p. e74421

Synchrotron FTIR microspectroscopy of Escherichia coli at single-cell scale under silver-induced stress conditions

Claire Saulou, Frederic Jamme, Laurence Girbal, Claude Maranges, Isabelle Fourquaux, Muriel Cocaign-Bousquet, Paul Dumas, and Muriel Mercier-Bonin

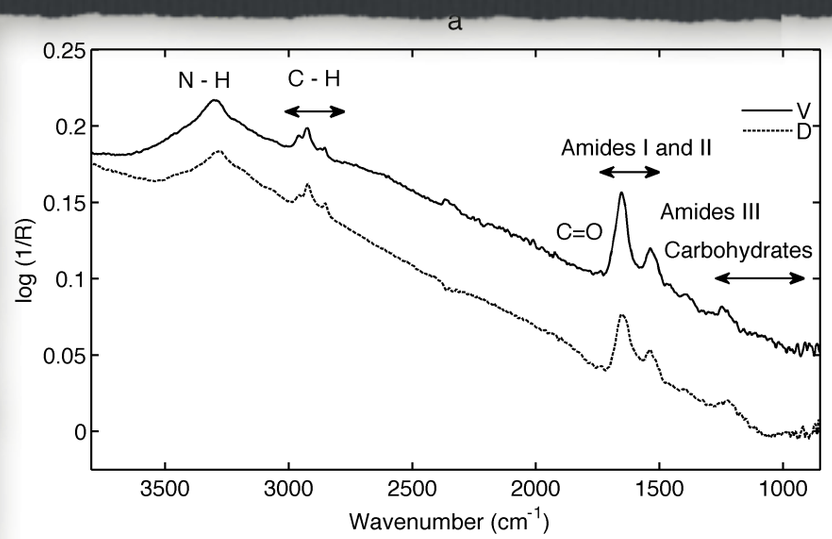


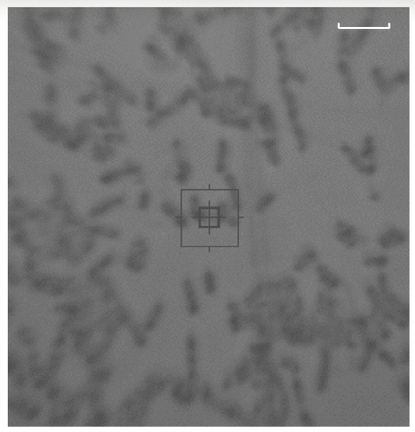


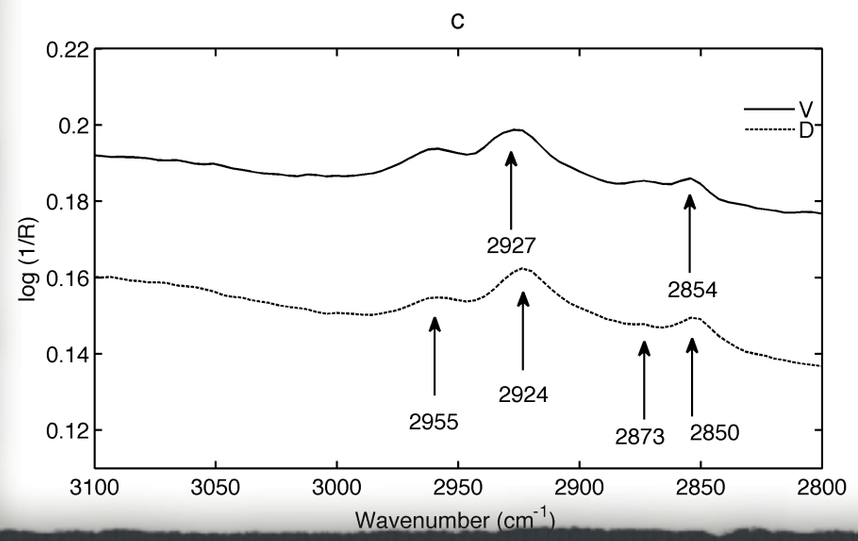
The present work was focused on elucidating biochemical changes in the model bacterium Escherichia coli exposed to ionic silver mediated stress, at a single-cell scale. In order to achieve this, in situ synchrotron Fourier-transform infrared (sFTIR) microspectroscopy was per- formed, for the first time, on individual cells by attenuated total reflectance (ATR) combined with the use of zinc- selenide hemisphere for high spatial resolution.

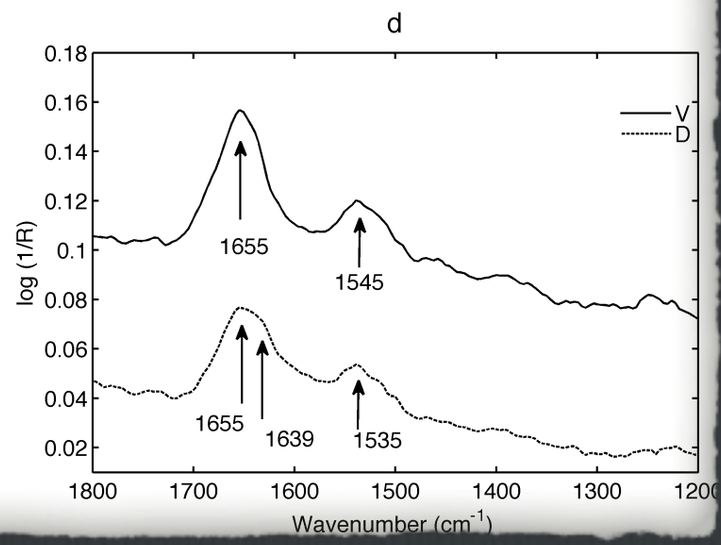
Anal Bioanal Chem 2013, vol. 405, pp. 2685 - 2697

Synchrotron FTIR microspectroscopy of Escherichia coli at single-cell scale under silver-induced stress conditions







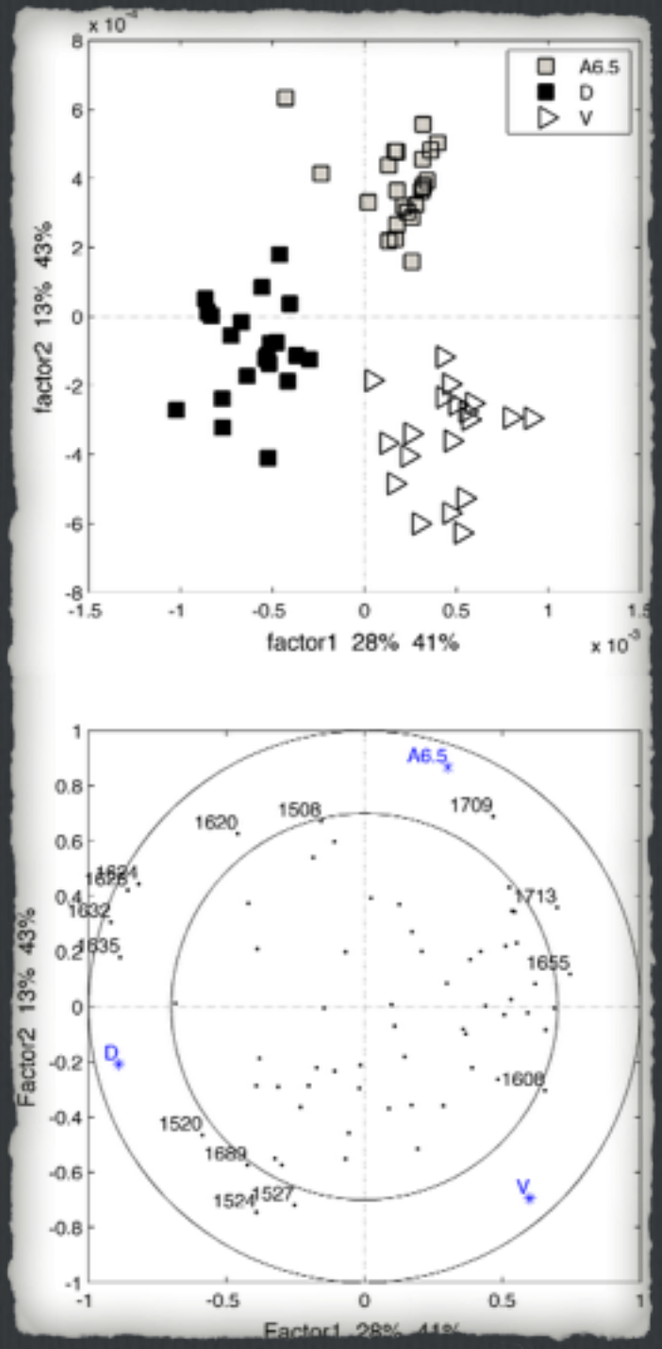


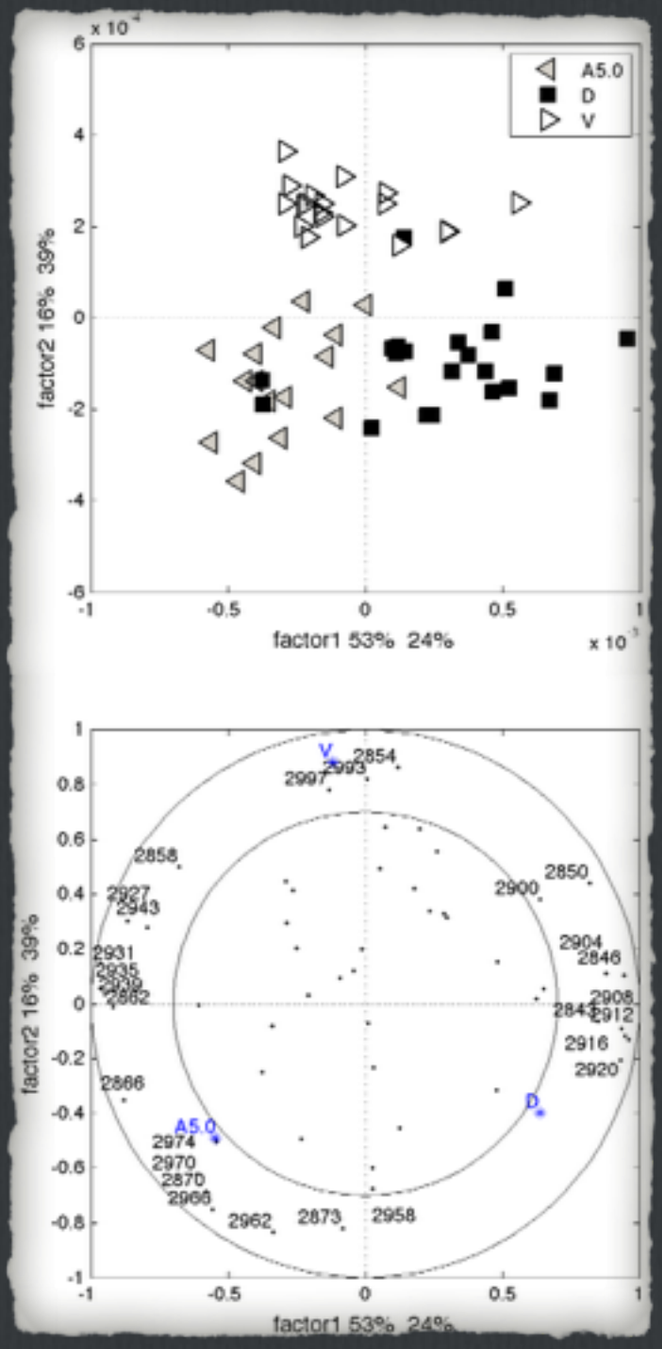
Differences in cell composition were assessed for the C–H stretching and protein spectral regions, indicating that the inhibitory action was targeted against both fatty acids and proteins. Transmission electron microscopy (TEM) confirmed morphological damages of the cell ultrastructure.

The relevance of ATR-sFTIR microspectroscopy for highlighting the heterogeneity in Ag^{+}-mediated effects within a given bacterial population was also pointed out. I

Anal Bioanal Chem 2013, vol. 405, pp. 2685 - 2697

Synchrotron FTIR microspectroscopy of Escherichia coli at single-cell scale under silver-induced stress conditions





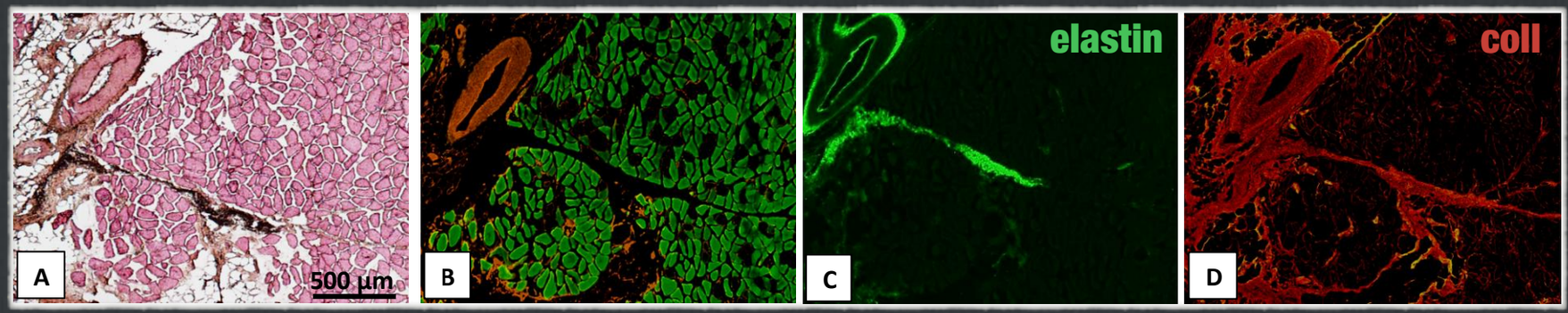
In the amide I and amide II region (1,700–1,480 cm^{-1}), the for group A6.5 (i.e. concentration of 6.5 μM $AgNO_3$), which was discriminated from the cluster V but did not overlap the cluster D . It should yet be noticed that group A6.5 was anti-correlated to the wavenumbers around 1,630 cm^{-1} and those around 1,525–1,520 cm^{-1}. This dem- onstrates that the secondary structure of proteins for cells submitted to “mild” silver-stress conditions was not as disordered as that of dead bacteria, although substantial biochemical differences were assessed compared to 100 % viable cells Effects were not significantly accentuated in the case of bacteria subjected to 8.5 μM $AgNO_3$.

In the 3,010–2,800-cm^{-1} range, treated bacteria showed an “intermediate” behaviour compared with 100 % viable (V) and dead (D) cells. The cluster corresponding to bacteria subjected to 5.0 μM $AgNO_3$, named A5.0, was well discriminated from group V . Some spectra were even close to group D

Anal Bioanal Chem 2013, vol. 405, pp. 2685 - 2697

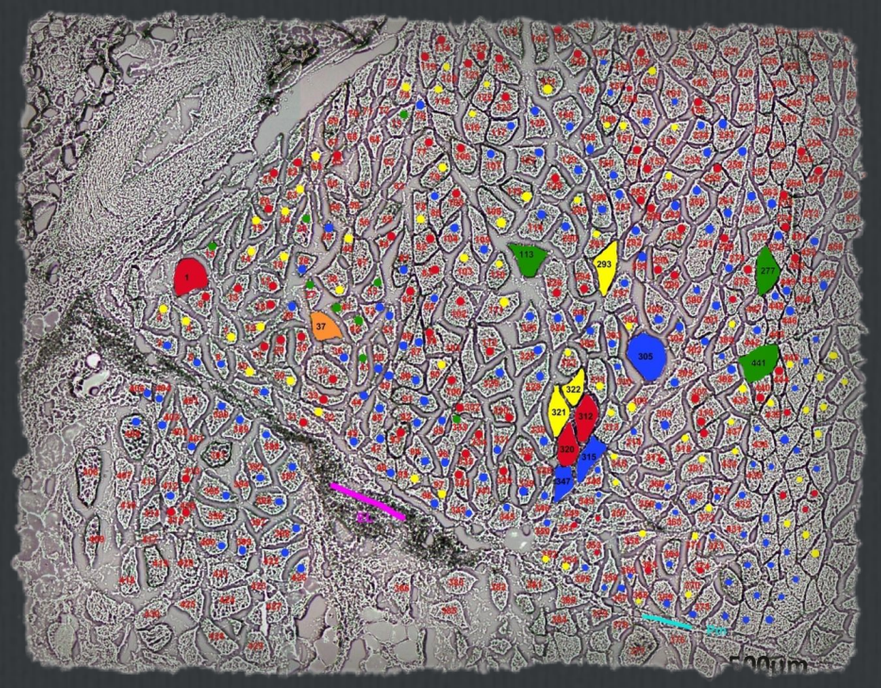
In situ thermal denaturation of myofibre sub-type proteins studied by immunohistofluorescence and synchrotron radiation FT-IR microspectroscopy

Thierry Astruc , Frédéric Peyrin , Annie Vénien, Roland Labas , Magali Abrantes , Paul Dumas , Frédéric Jamme



The thermal denaturation of proteins in skeletal muscle was studied and characterised taking into account the in situ metabolic and contractile fibre types. From serial histological sections, collagen, elastin, various type I, IIa and IIx fibres and type I–IIa and IIa–IIx hybrids were identified by immunohistofluorescence.

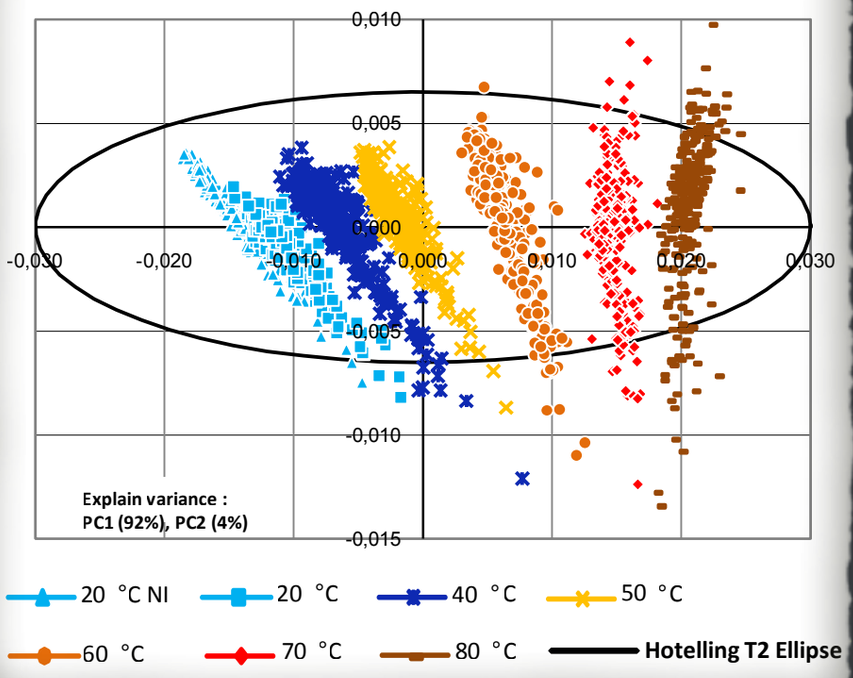
Histological sections were incubated in buffer solutions at increasing temperatures (40, 50, 60, 70 and 80 °C).

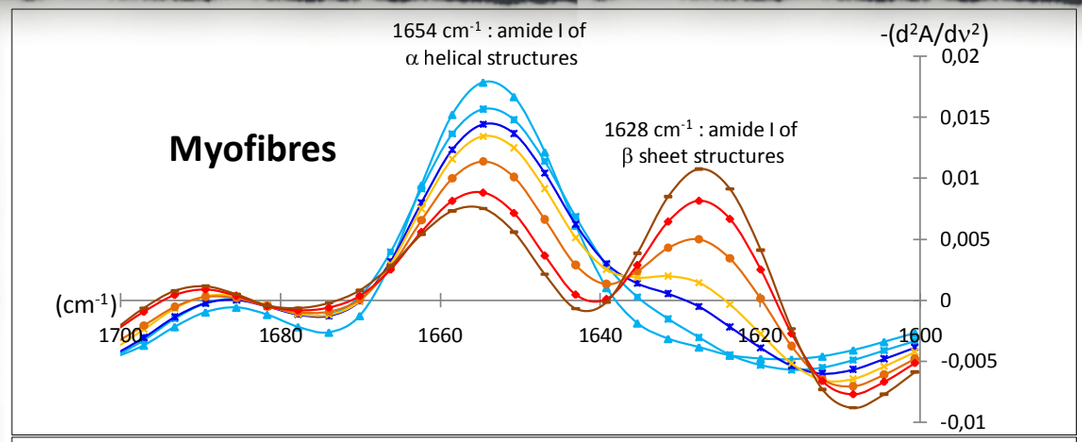


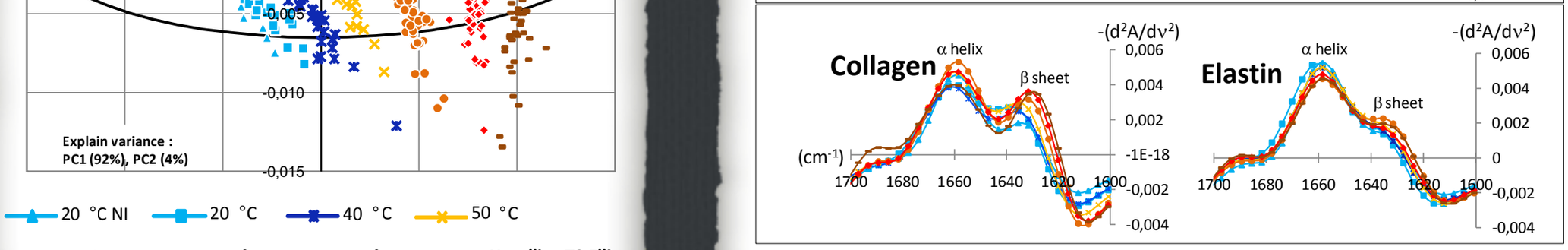
Food Chemistry 2012, vol. 134, p. 1044–1051

In situ thermal denaturation of myofibre sub-type proteins studied by immunohistofluorescence and synchrotron radiation FT-IR microspectroscopy

Principal Component Analysis of myofibre negative second derivative spectra. PC1 vs PC2 scores at 1700-1600 cm^{-1}





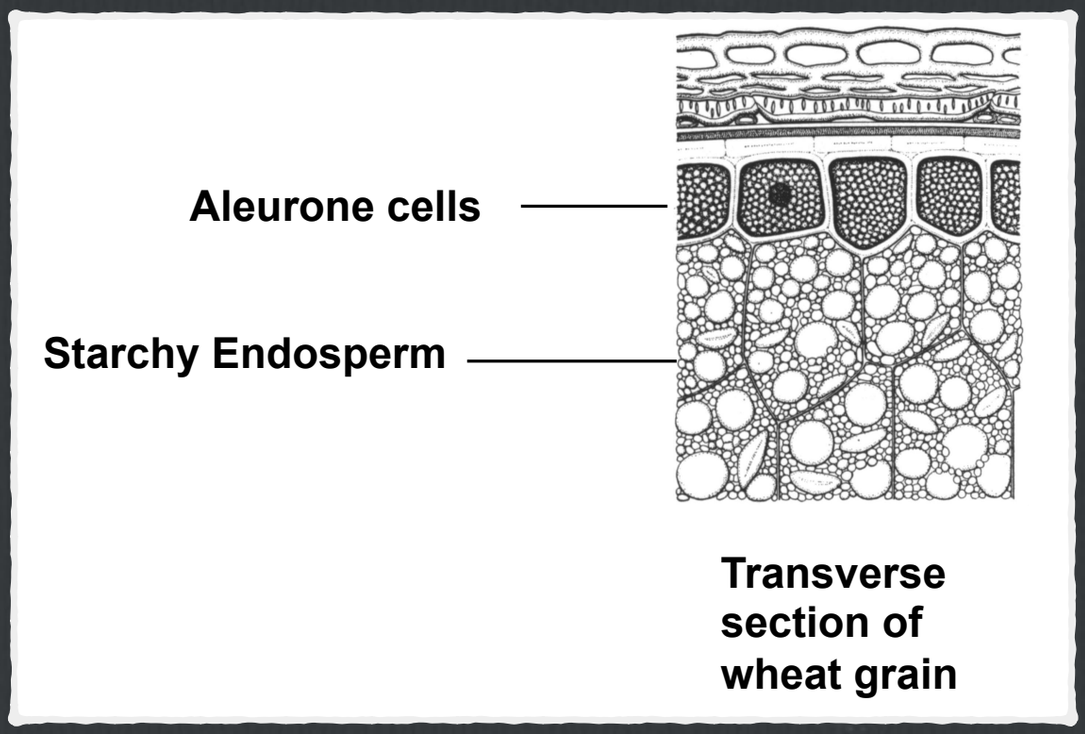


Using FT-IR microspectroscopy made it possible to characterise the secondary structure of proteins directly on sections of muscle tissue that have not undergone any chemical treatment and have thus preserved their molecular assemblies. The secondary structure of collagen is significantly altered from 60 °C, whereas the secondary structure of elastin remains relatively stable until 80 °C. The secondary structure of myofibrillar protein clearly changes according to heating temperature, but no significant differences between fibre types were found, suggesting that proteins still bound by their molecular interactions demonstrate better thermal stability.

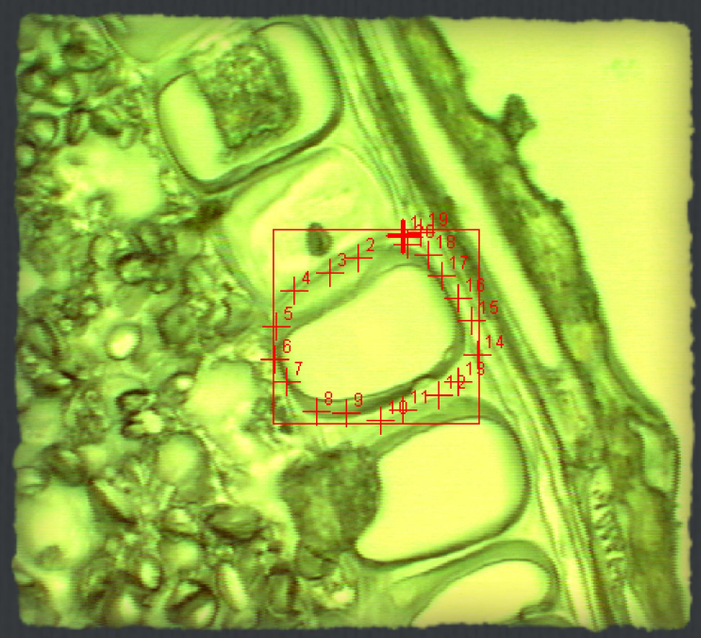
Food Chemistry 2012, vol. 134, p. 1044–1051

Aleurone cell walls of wheat grain: high spatial resolution investigation using synchrotron infrared microspectroscopy

F. Jamme, P Robert, B Bouchet, L Saulnier, P Dumas, F Guillon



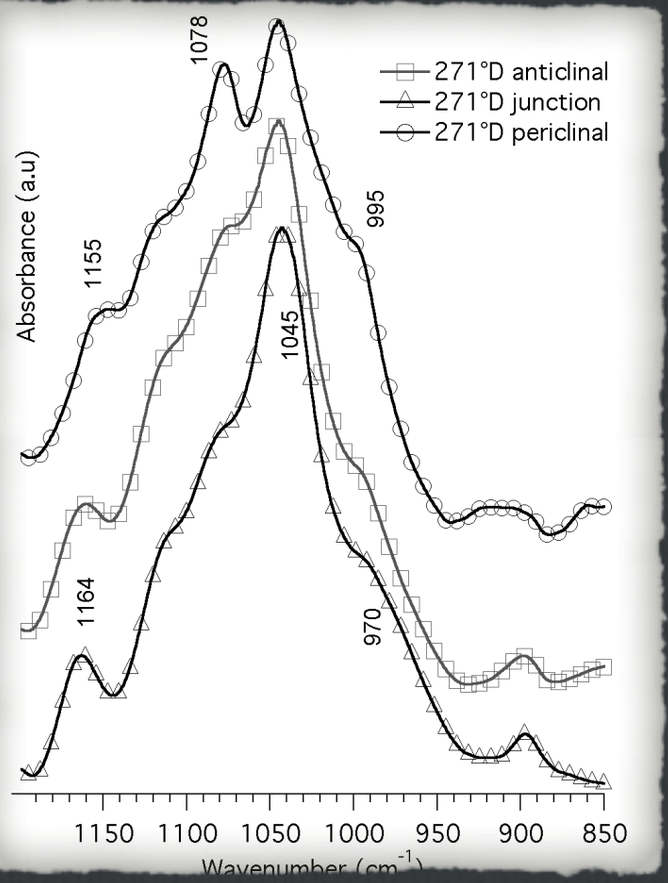
Transverse section of wheat grain

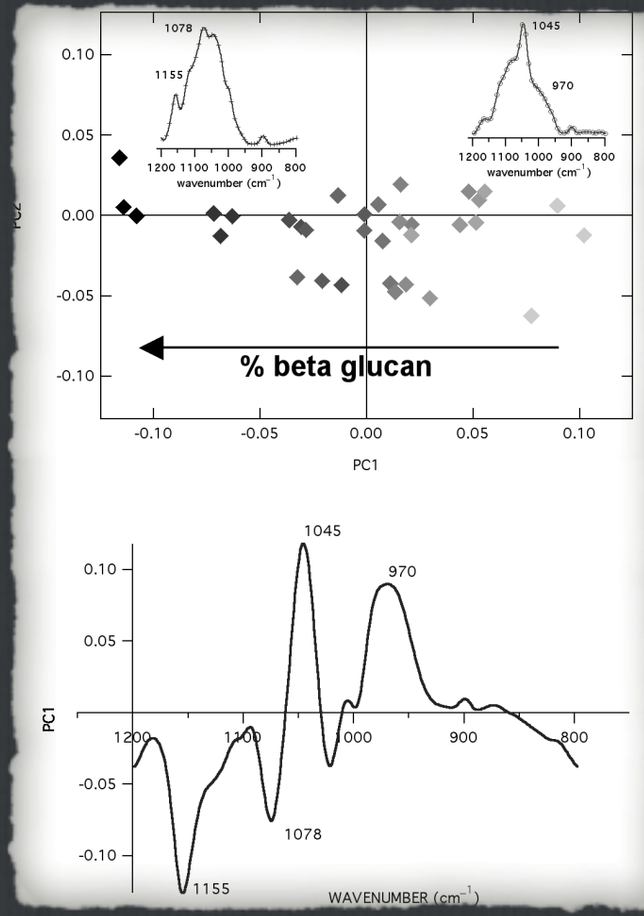


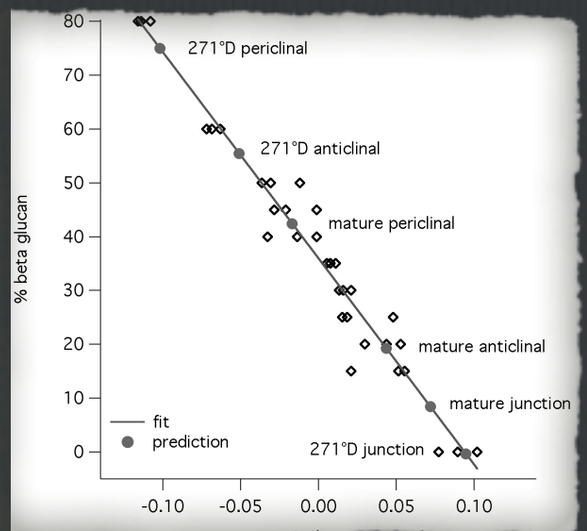
Infrared microspectroscopy and immunolabeling techniques were employed in order to obtain deeper insight into the biochemical nature of aleurone cell walls of wheat grain. The use of a synchrotron source, thanks to its intrinsic brightness, has provided unprecedented information at the level of a few micrometers and has allowed the discrimination of various polysaccharides in cell walls. The high spectral quality obtained in the small analyzed domain has been beneficial in estimating the relative proportions of beta-glucan and arabinoxylan, through the use of principal component analysis (PCA).

Applied Spectroscopy, 2008, vol . 62(8) pp. 895-900

Aleurone cell walls of wheat grain: high spatial resolution investigation using synchrotron infrared microspectroscopy







For each stage of grain development, the spectra were classified in 3 groups of cell wall region: anticlinal, junction and periclinal as shown in the previous slide. About 50 spectra per cell wall region and per stage of development were recorded. Mean spectra were assessed for each cell wall region and each stage of development.

The infrared spectra of the aleurone layer were projected into the PCA space created from the model mixtures. The percentage of glucan was therefore estimated by applying the equation of prediction previously assessed by linear regression.

Applied Spectroscopy, 2008, vol . 62(8) pp. 895-900

DISCO beamline team



Journal of Synchrotron Radiation 2009, vol. 16, 835–841.

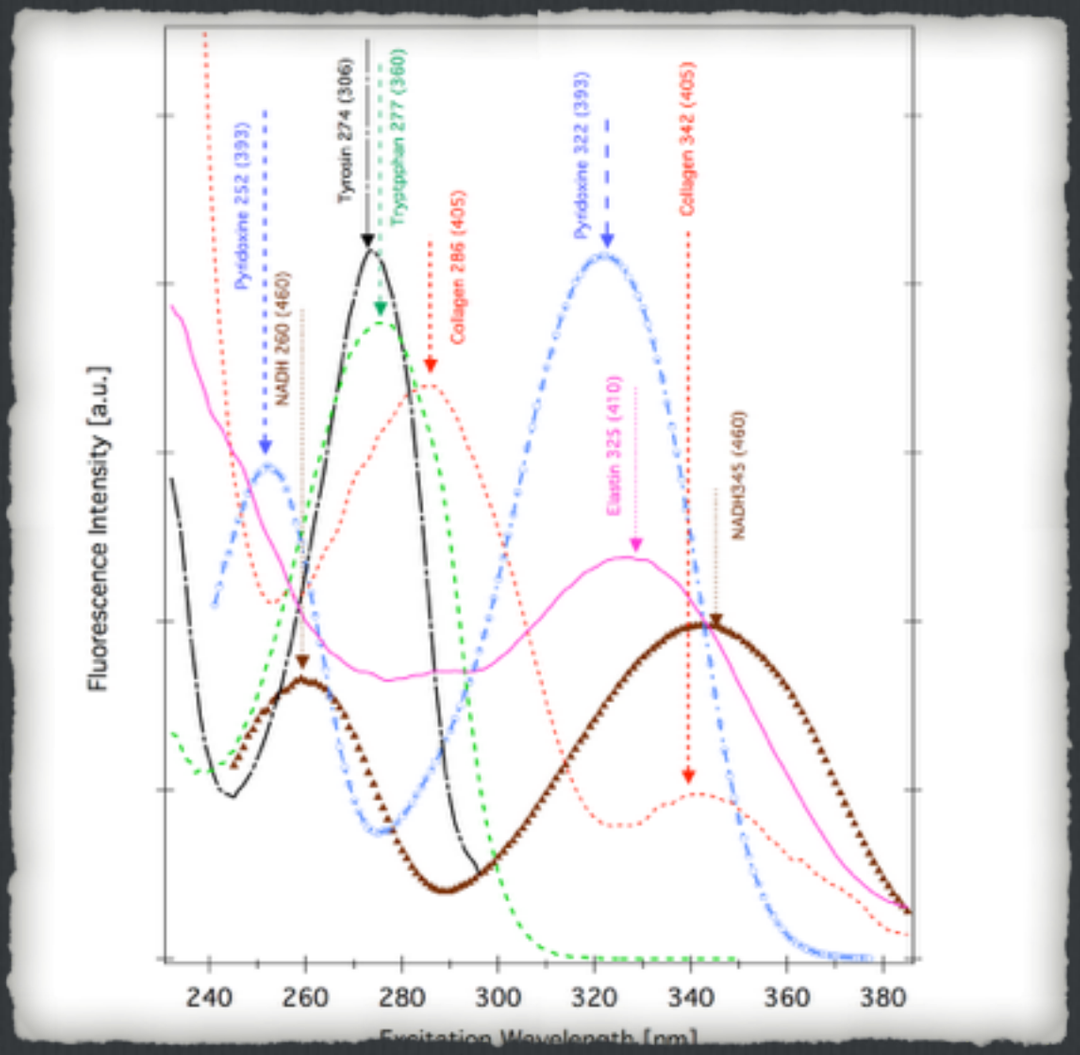
DISCO
DUV 200-350 nm

ZnO TiO2

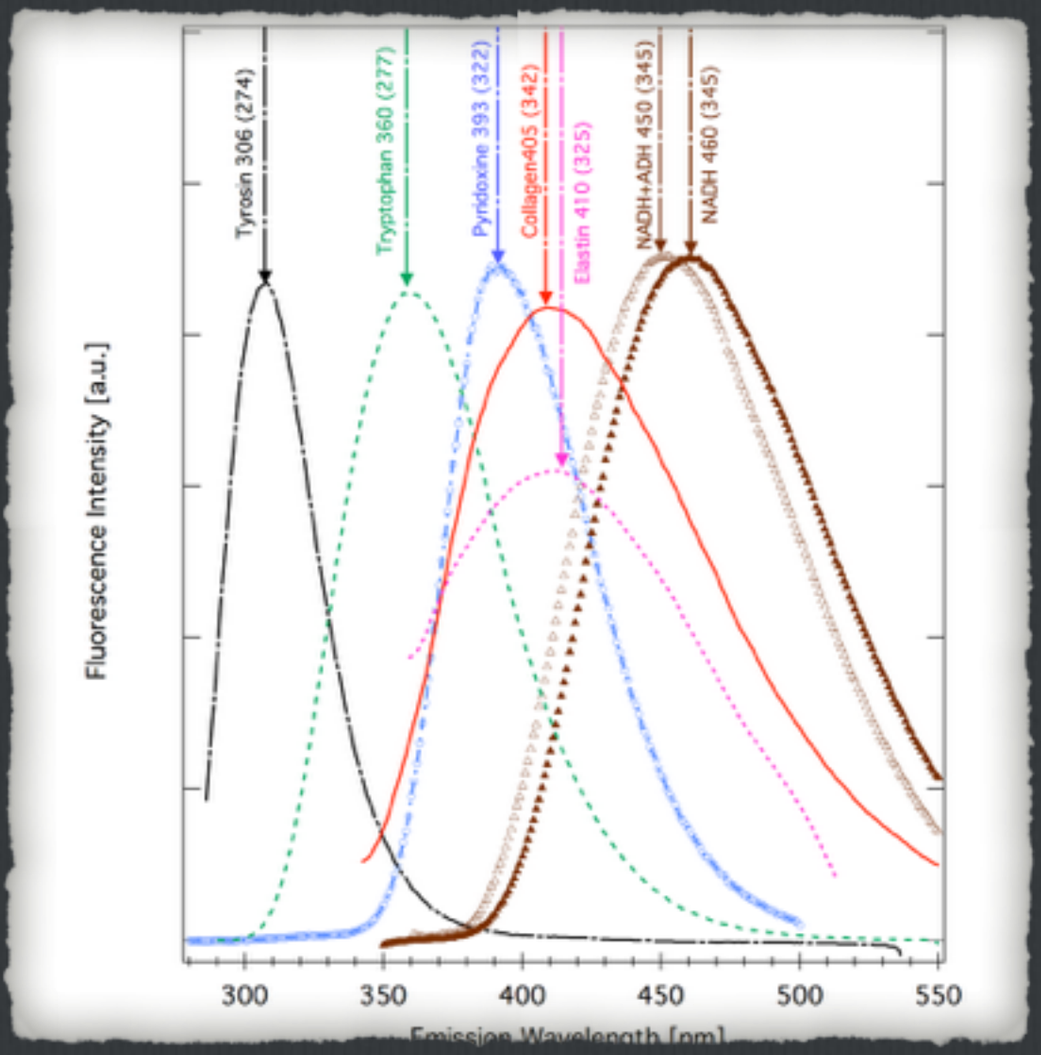
Tryp. coll. NADH

Tyr. Elastin

☐ Excitation



☐ Emission

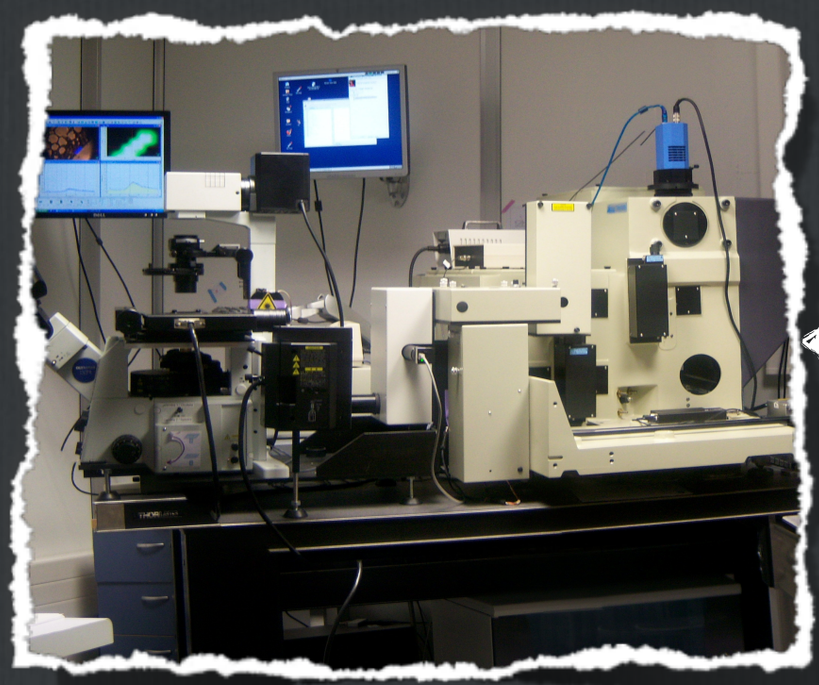


Biology of the Cell 2013, vol. 105, 277–288.

DISCO IMAGING
DUV 200-350 nm

POLYPHEME

TELEMOS

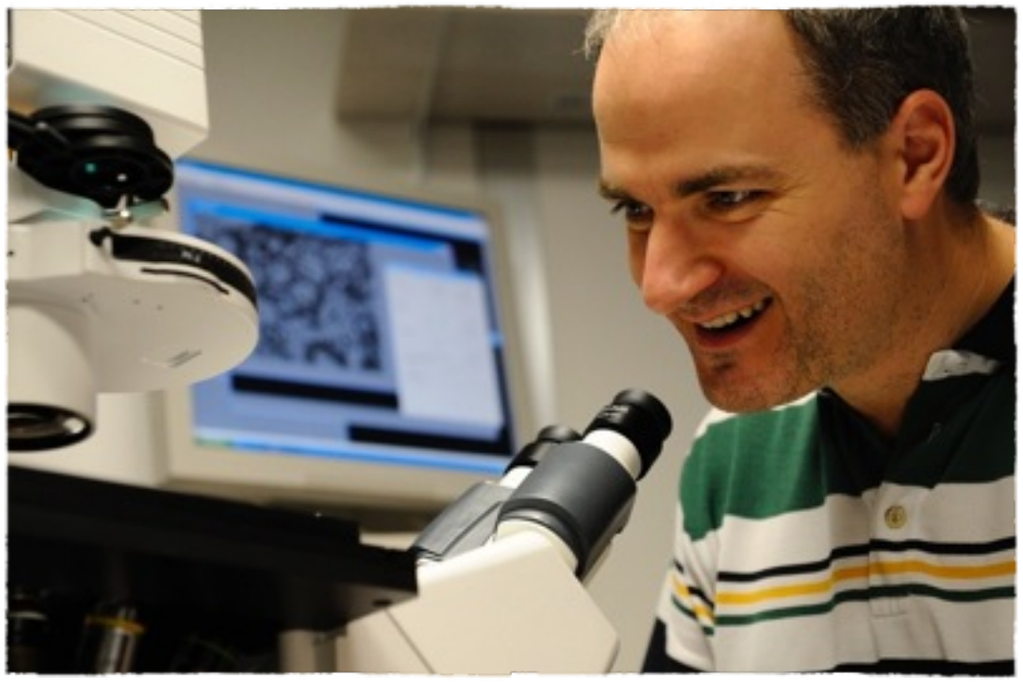






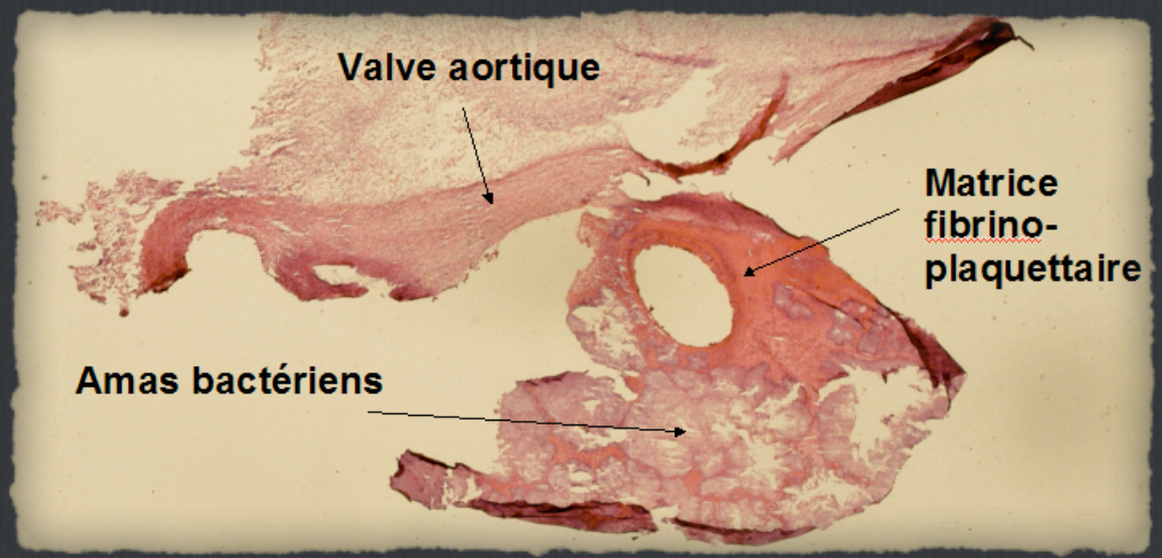
Microsc. Microanal. 2010, vol. 16, 507–514.

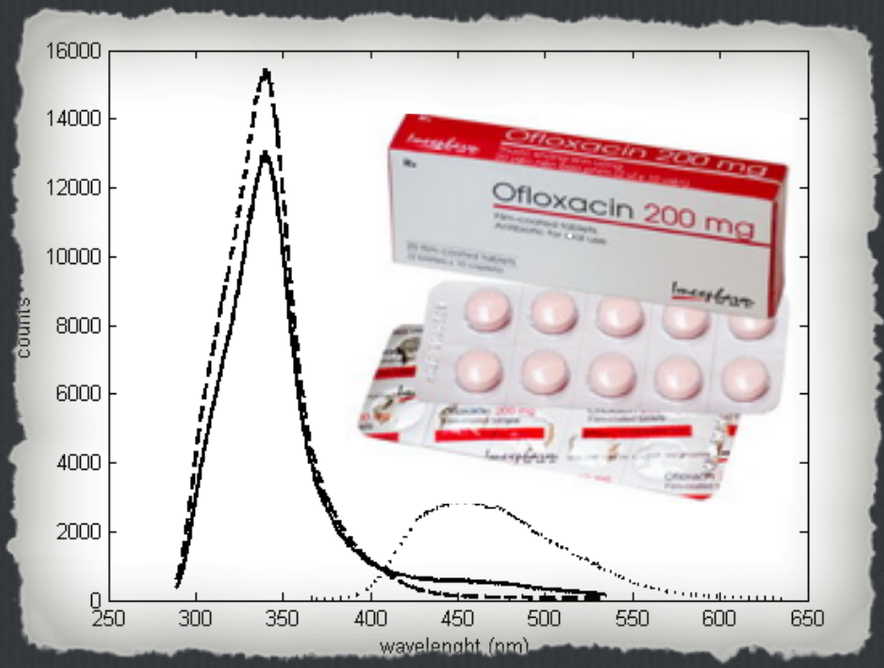
DISCO Highlights



Diffusion of Ofloxacin in the Endocarditis Vegetation Assessed with Synchrotron Radiation UV Fluorescence Microspectroscopy

Batard, E., Jamme, F., Villette, S., Jacqueline, C., de la Cochetière, M. F., Caillon, J., & Réfregiers

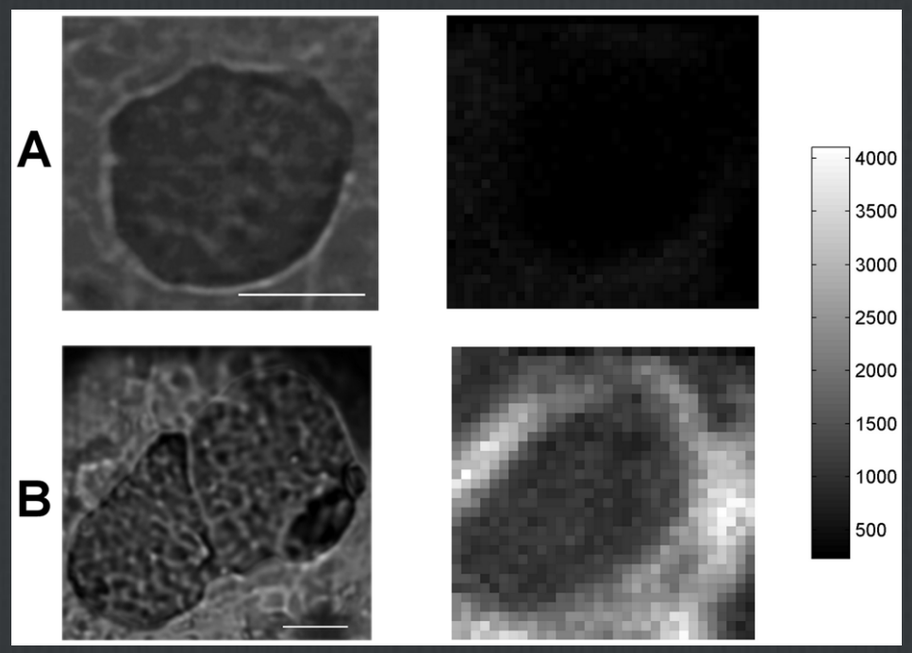




The objective of this work was to assess the diffusion of ofloxacin in experimental endocarditis vegetation bacterial masses using synchrotron-radiation UV fluorescence microspectroscopy. Two fluorescence microscopes were coupled to a synchrotron beam for excitation at 275 nm. A spectral microscope collected fluorescence spectra between 285 and 550 nm. A second, full field microscope was used with bandpass filters at 510–560 nm. Spectra of ofloxacin-treated vegetations presented higher fluorescence between 390 and 540 nm than control.

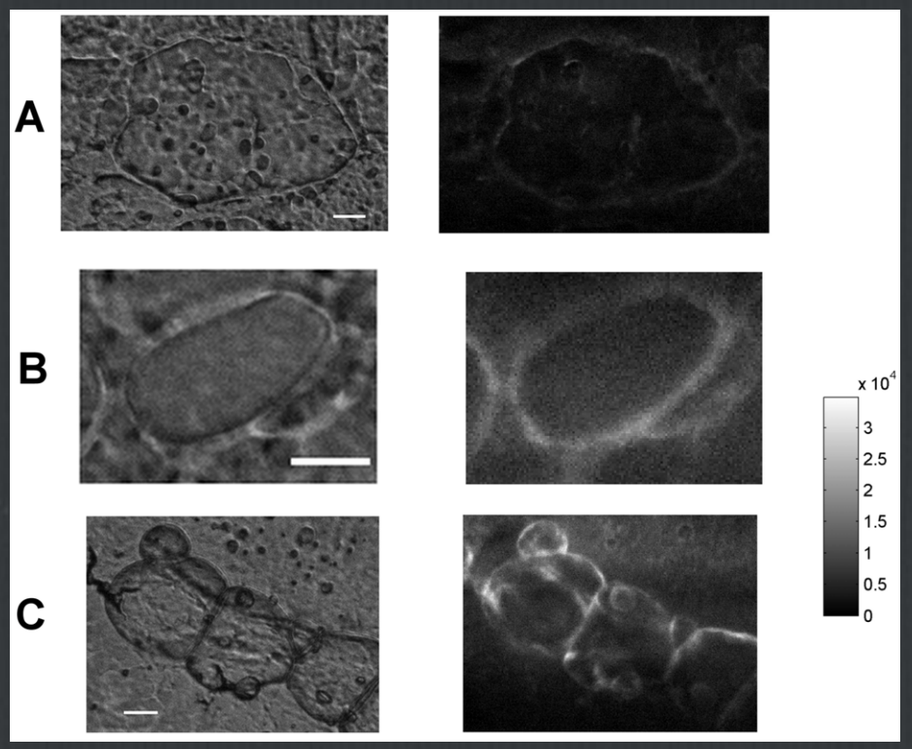
PLoS One, 2011, 6(4): art.n° e19440

Diffusion of Ofloxacin in the Endocarditis Vegetation Assessed with Synchrotron Radiation UV Fluorescence Microspectroscopy



Full field imaging showed that ofloxacin increased fluorescence between 510 and 560 nm. Ofloxacin diffused into vegetation bacterial masses, although it accumulated in their immediate neighborhood. Fluorescence images additionally suggested an ofloxacin concentration gradient between the vegetation peripheral and central areas.

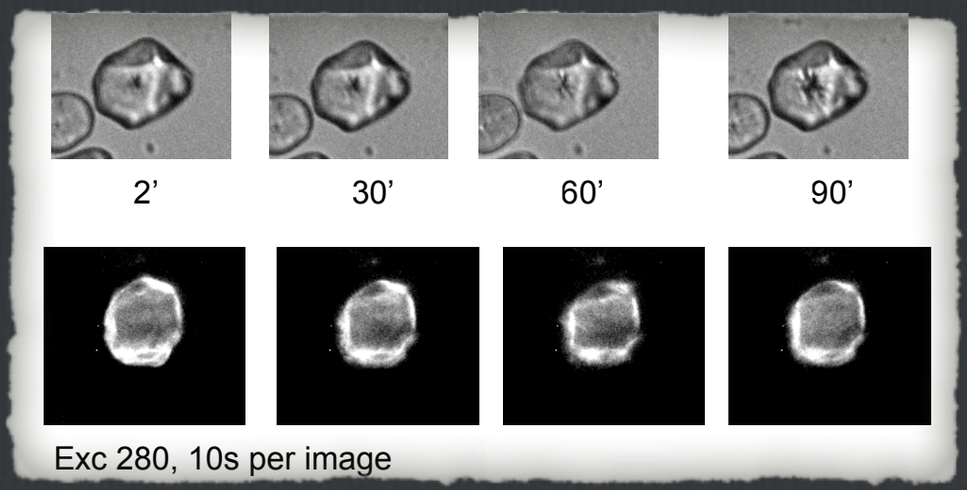
In conclusion, ofloxacin diffuses into vegetation bacterial masses, but it accumulates in their immediate neighborhood. Synchrotron radiation UV fluorescence microscopy is a new tool for assessment of antibiotic diffusion in the endocarditis vegetation bacterial masses.



PLoS One, 2011, 6(4): art.n° e19440

In situ tracking of enzymatic breakdown of starch granules by synchrotron UV fluorescence microscopy

Tawil, G., Jamme, F., Réfregiers, M., Viksø-Nielsen, A., Colonna, P., & Buléon, A.



Top: Visible light imaging of maize starch granules during hydrolysis by AFA at different stages of hydrolysis (from 1 to 90 min
Bottom: : Fluorescence images of amylase adsorption on maize starch granules during hydrolysis by AFA (lexcitation 280 nm, recording time 10 s)

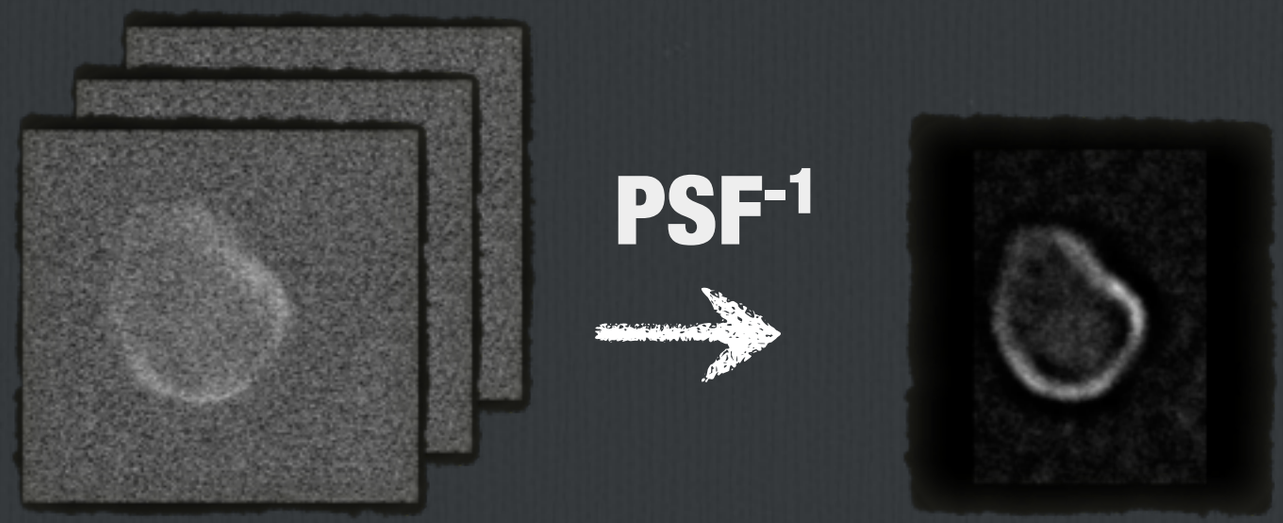
Synchrotron UV fluorescence microscopy was used for the first time to visualize the adsorption and diffusion of a degrading enzyme on its solid substrate. The degradation pathway of single starch granules by two amylases (RA and AFA), optimized for biofuel production and industrial starch hydrolysis, was followed by tryptophan fluorescence (excitation at 280 nm, emission filter at 300-400 nm) and visible light imaging.



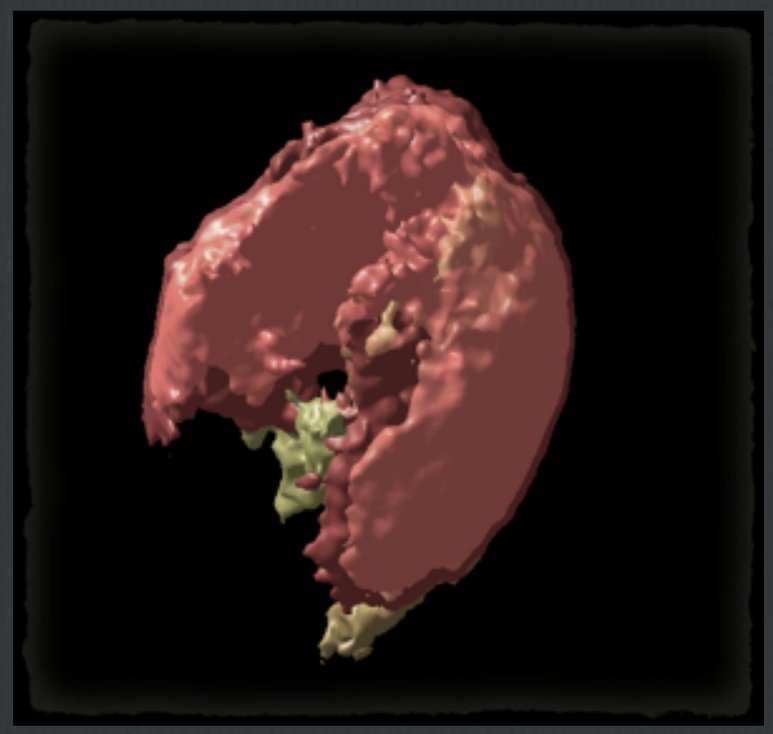
Analytical Chemistry, 2011, 83(3): 989–993

In situ tracking of enzymatic breakdown of starch granules by synchrotron UV fluorescence microscopy

Using automated Z collection, we are able to record z stacks of studied sample. Thus, TELEMOS PSF (Point spread function) is estimated and PSF deconvolution applied (Huygens software, SVI, NI)



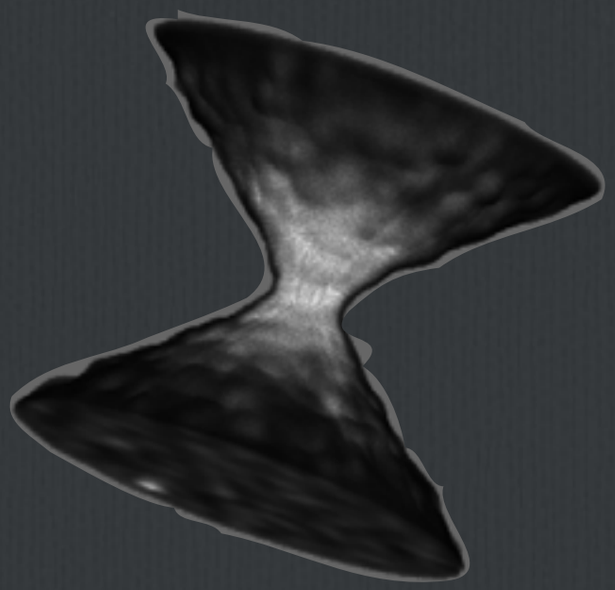
2D stack



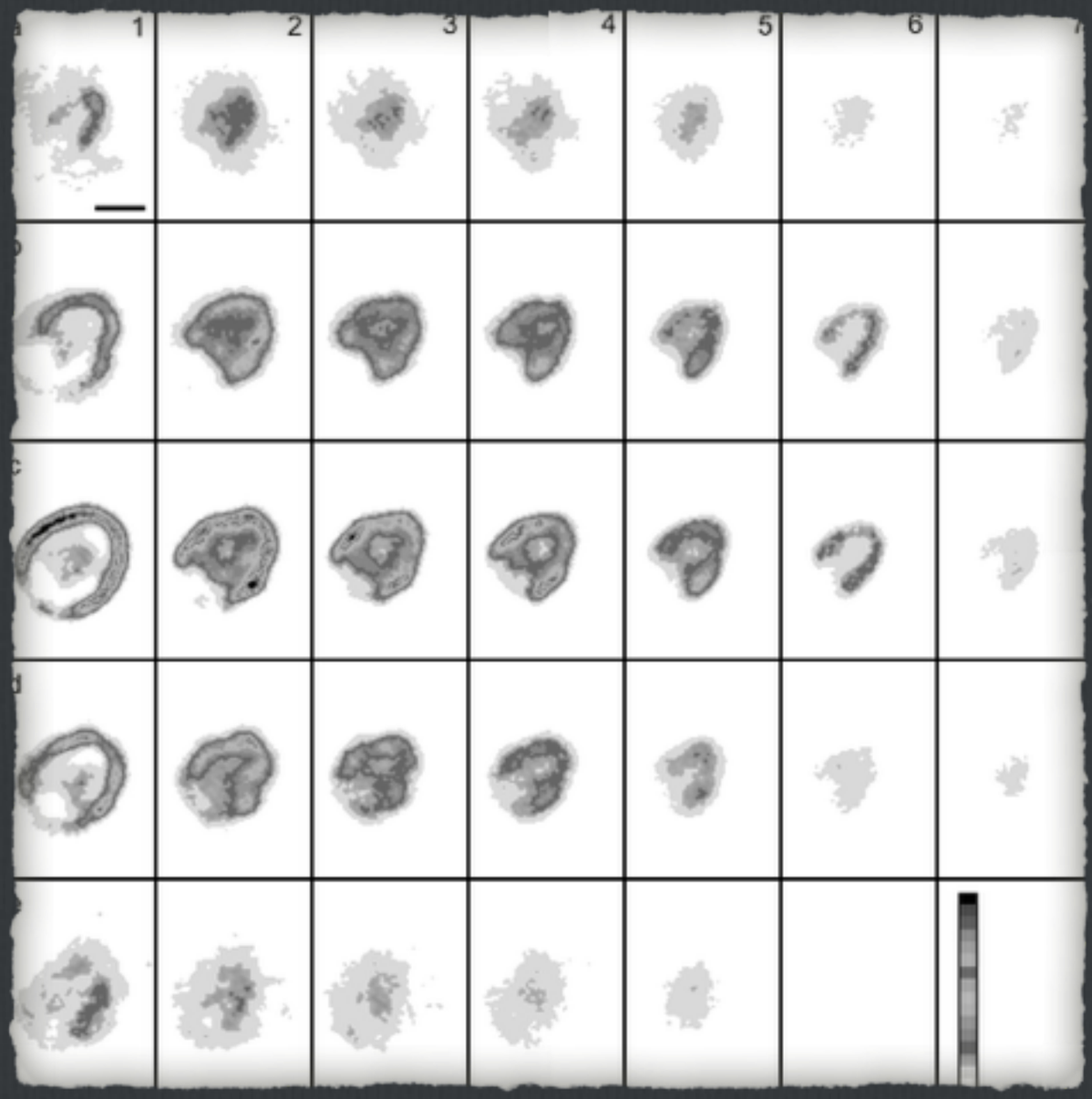
3D reconstruction

Analytical Chemistry, 2013, submitted

In situ tracking of enzymatic breakdown of starch granules by synchrotron UV fluorescence microscopy







The present work describes challenging new improvements of the technique including especially multi-Z acquisition and subsequent 3D image building and their application to hydrolysis of maize starch granules by RA and AFA allowing to image in 3D the diffusion of these enzymes within the internal parts of starch granules all along their hydrolysis.

Analytical Chemistry, 2013, submitted

Synchrotron UV fluorescence microscopy to determine membrane fluidity modification of single bacteria with temperatures

Stéphanie Passot, Frédéric Jamme , Matthieu Réfrégiers, Julie Gautier, Stéphanie Cenard, Fernanda Fonseca



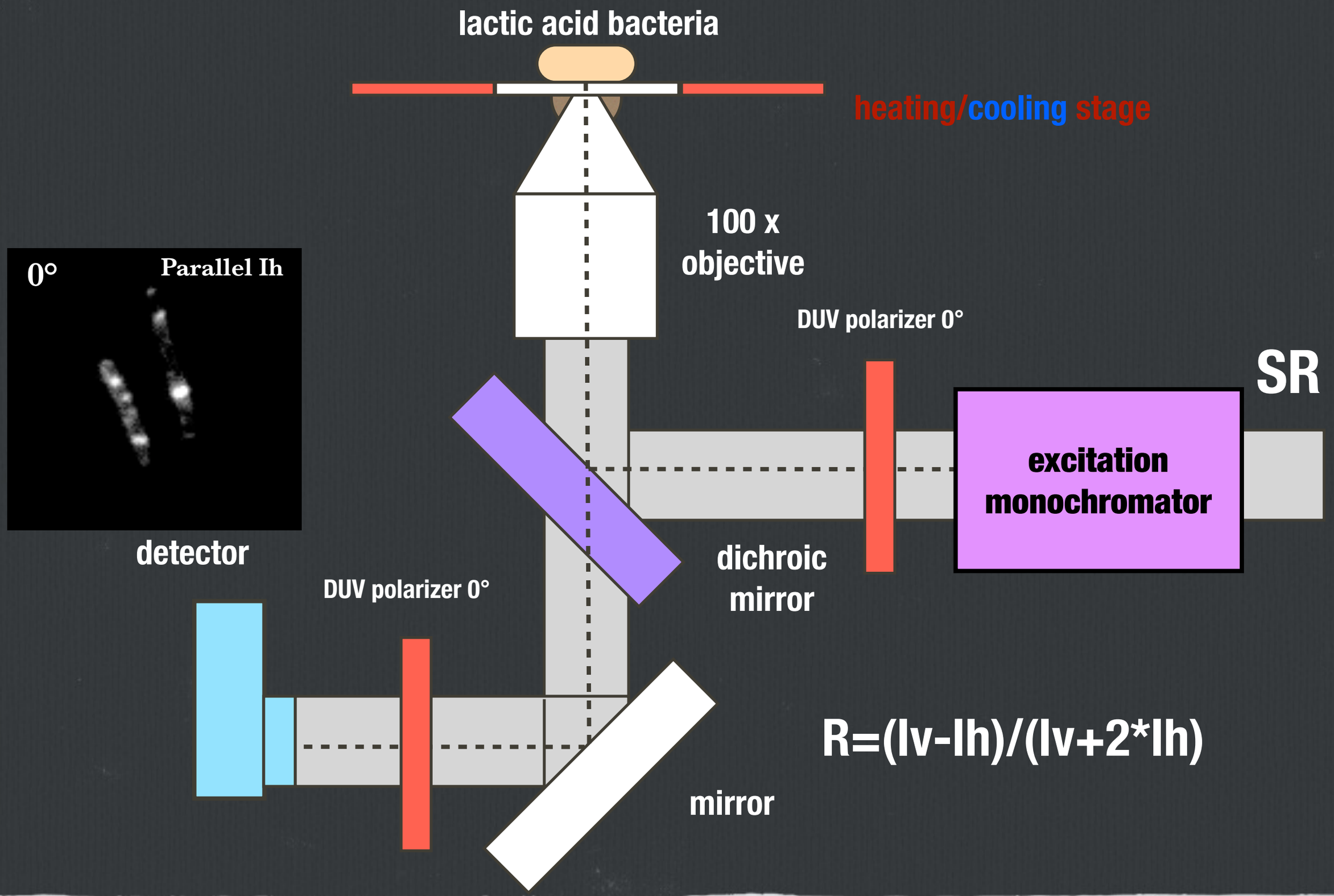
Using analogs of cholesterol (TMA-DPH) as probes of membrane fluidity

Cryopreservation of bacteria requires specific cells pre-adaptation as well as controlled freezing protocol to minimize membrane damage resulting from osmotic dehydration. Membrane fluidity has thus an important role in biophysical events taking place at subzero temperatures, facilitating or not the exchanges between intracellular and extracellular media. An original approach using Synchrotron fluorescence polarization microscopy was developed to measure membrane fluidity of single bacteria. Cells were labelled with the cytoplasmic membrane probe trimethylammoniumdiphenylhexatriene (TMA-DPH). The degrees of liberty of TMA-DPH inside the bilayer provide a direct marker of membrane fluidity under DUV excitation.

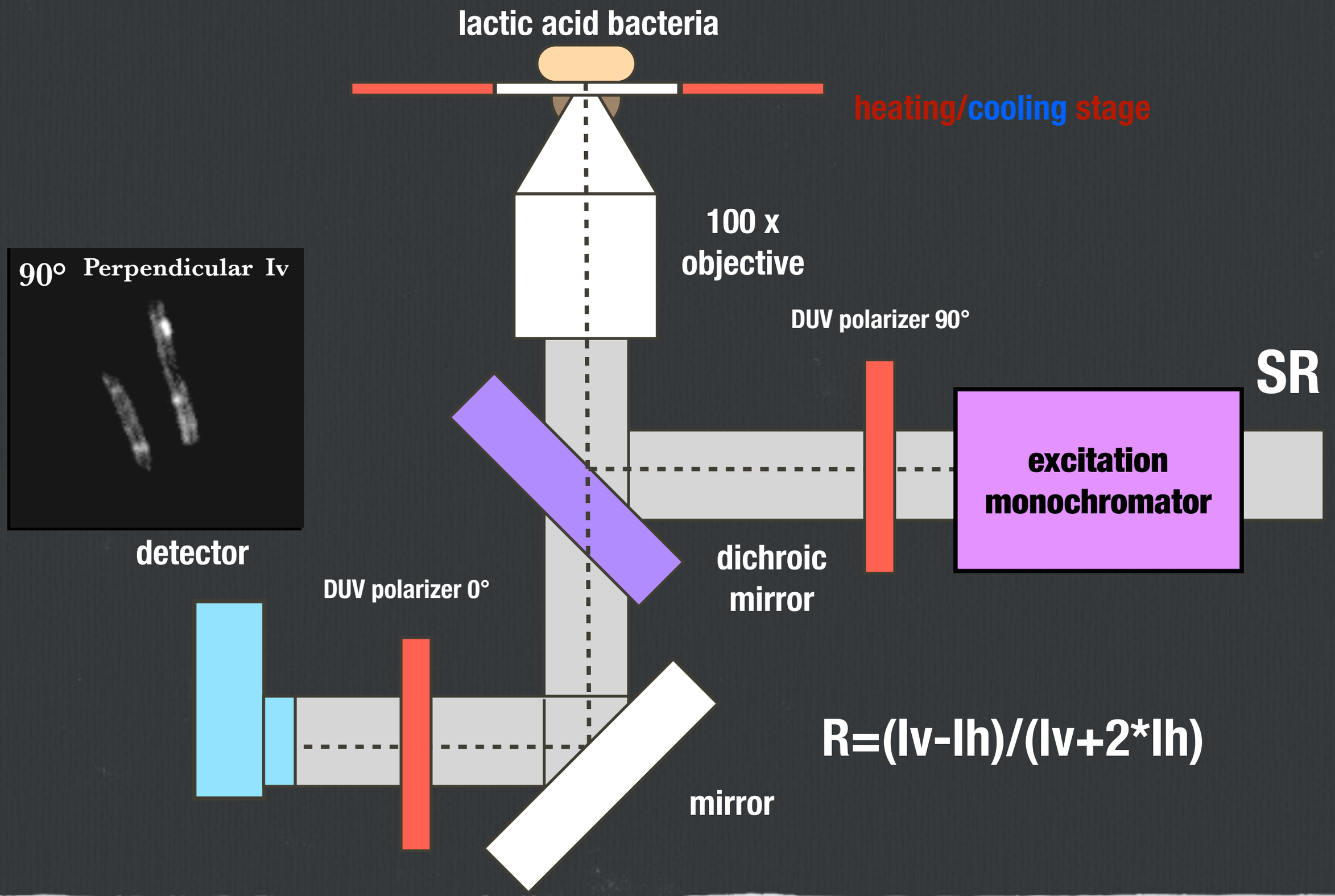
Couples of fluorescence polarization images from zero to forty degrees were recorded by inserting polarizers into the excitation and emission paths. The fluorescence anisotropy of the images was calculated allowing the assessment of the membrane fluidity. Results indicate intercellular and intracellular heterogeneities with subdomains appearing at low temperature.

Biomedical Spectroscopy and Imaging, 2013, ECSBM proceedings , in print

Synchrotron UV fluorescence microscopy to determine membrane fluidity modification of single bacteria with temperatures

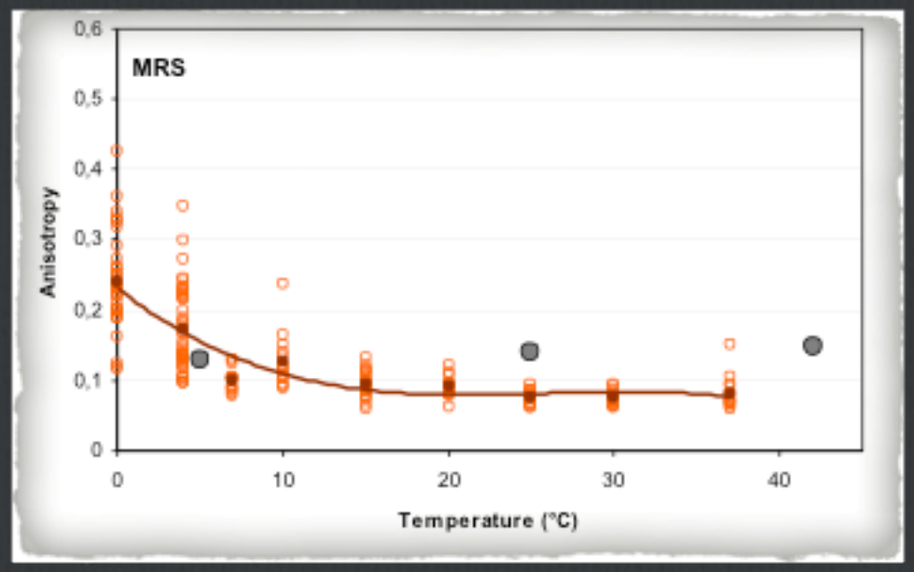


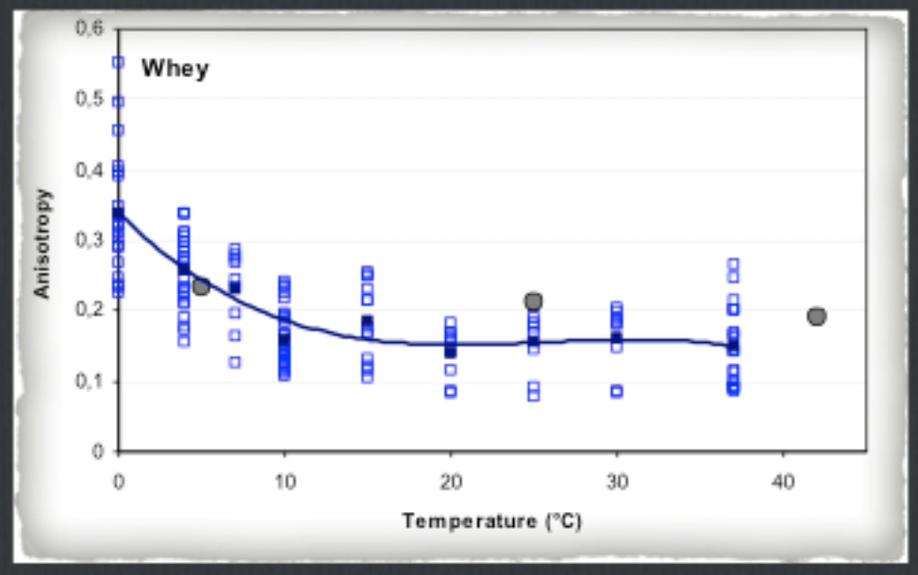
Synchrotron UV fluorescence microscopy to determine membrane fluidity modification of single bacteria with temperatures



Synchrotron UV fluorescence microscopy to determine membrane fluidity modification of single bacteria with temperatures

Stéphanie Passot, Frédéric Jamme , Matthieu Réfrégiers, Julie Gautier, Stéphanie Cenard, Fernanda Fonseca

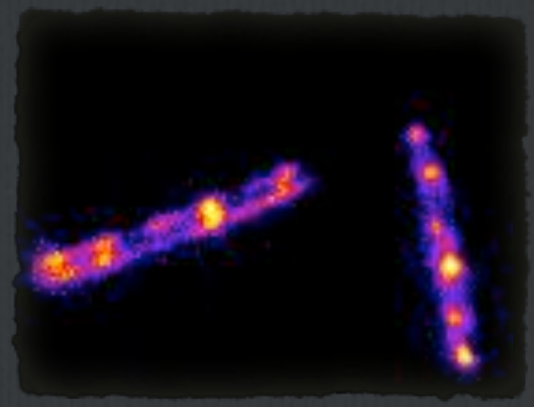




Membrane anisotropy behaviour of individual cells of Lb. bulgaricus CFL1 cultivated in MRS broth (A) and in mild whey medium (B) as a function of temperature determined by Synchrotron UV microscopy.

This is the first time that synchrotron DUV anisotropy measurement of bacteria membranes is performed. This technique measures individual bacteria membrane fluidity and emphasizes the inter-bacterial heterogeneities measured by flow cytometry.

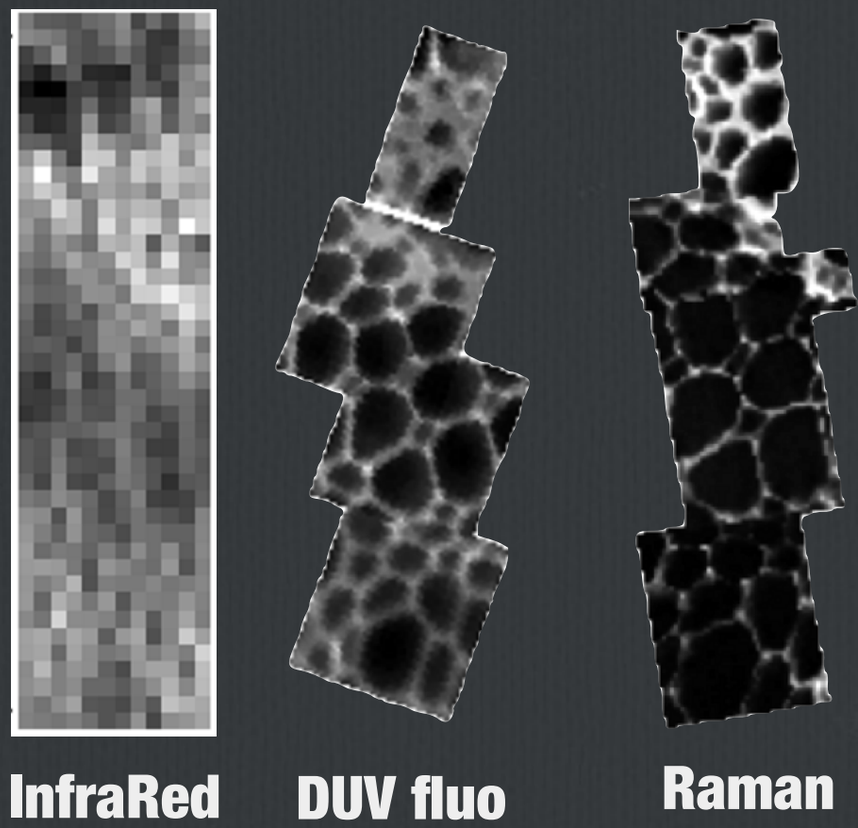
More strikingly, it demonstrates intracellular heterogeneities at low temperature with rigid domains that start to nucleate inside a still fluid bilayer at 4°C. In a near future, those results will be improved by pushing the temperature control at negative temperatures with a new Peltier device.



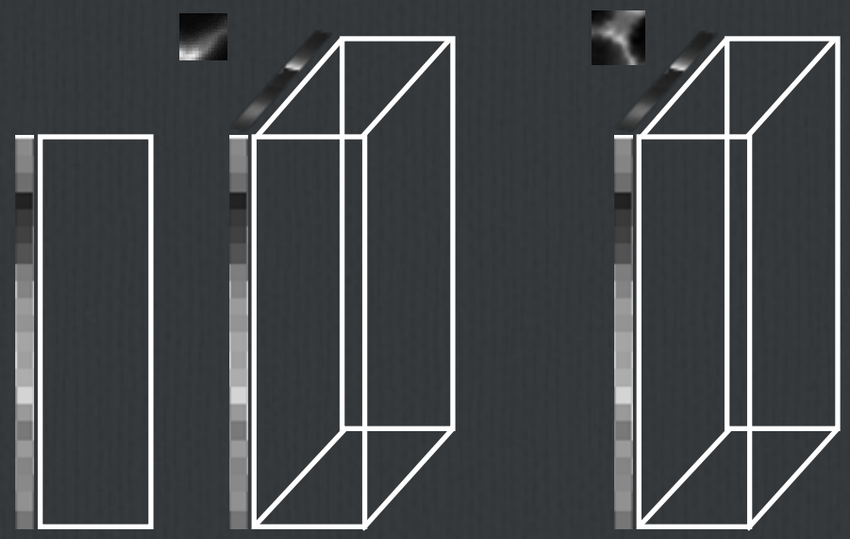
Biomedical Spectroscopy and Imaging, 2013, ECSBM proceedings , in print

Coupling Hyper Spectral Images
“CouplImSpec”

Allouche, F., Hanafi, M., Jamme, F., Robert, P., Barron, C., Guillon, F., and Devaux, M. F.



Multiblock analysis



$$Max \sum_{k=1}^{K} \mathrm{cov}^2(\mathbf{c}_{\mathrm{X}_k}, \mathrm{c}_{\mathrm{g}})$$

Chemometrics and Intelligent Laboratory Systems, 2012, vol. 117, pp. 200–212

X

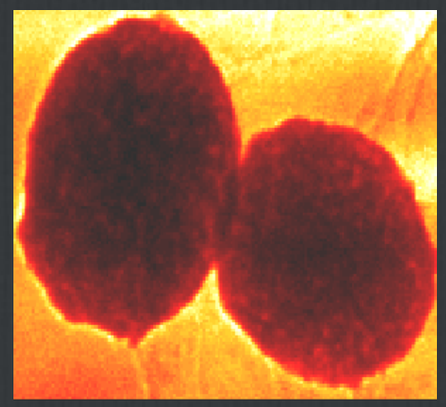
Absorption X

Imagerie absorption X

distribution (2D/3D) des caractéristiques/« contrastes » sondés par des interactions des rayons X avec la matière

résolution spatiale (μm)

Détecteur d'imagerie (2D)





échantillon

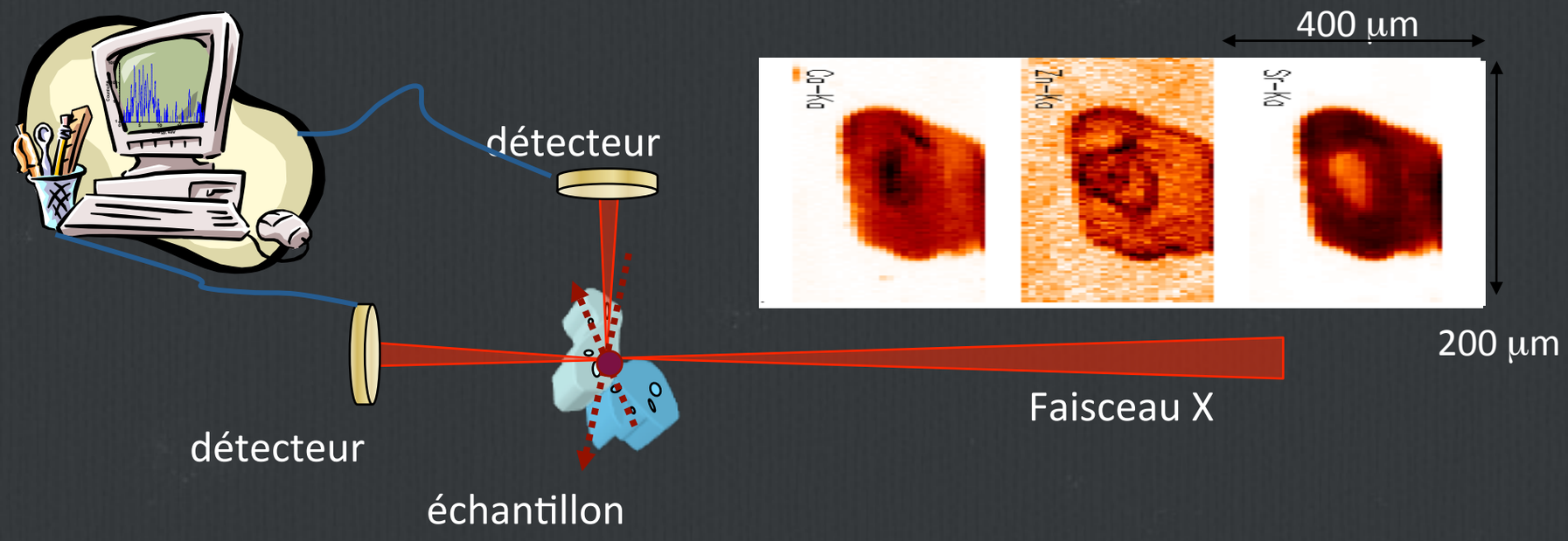
from Andrea SOMOGYI (synchrotron SOLEIL, Nanoscopium)

Absorption X

Imagerie X: distribution (2D/3D) des caractéristiques/« contrastes » sondés par des interactions des rayons X avec la matière

résolution spatiale

Dimension du faisceau
+balayage avec l'échantillon



from Andrea SOMOGYI (synchrotron SOLEIL, Nanoscopium)

Absorption X - Water window

Imagerie absorption X – Fenetre de l'eau

Fenêtre de l'eau: X-mous 284 eV< E_0 < 543 eV

(énergie d'ionisation des seuils K du C et O).

Absorption de matériaux avec une composition

du carbone >>> d'oxygène

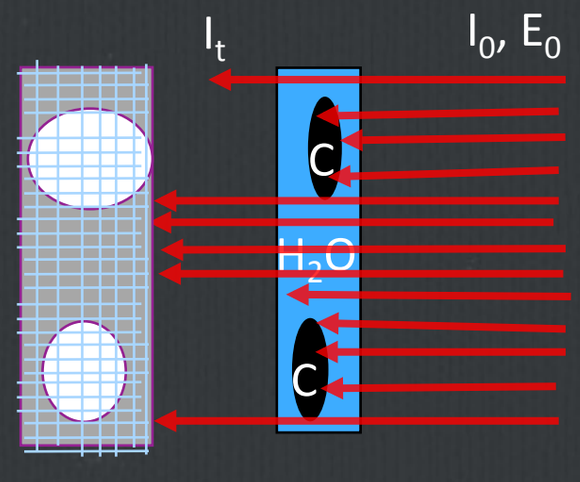
matériel organique eau

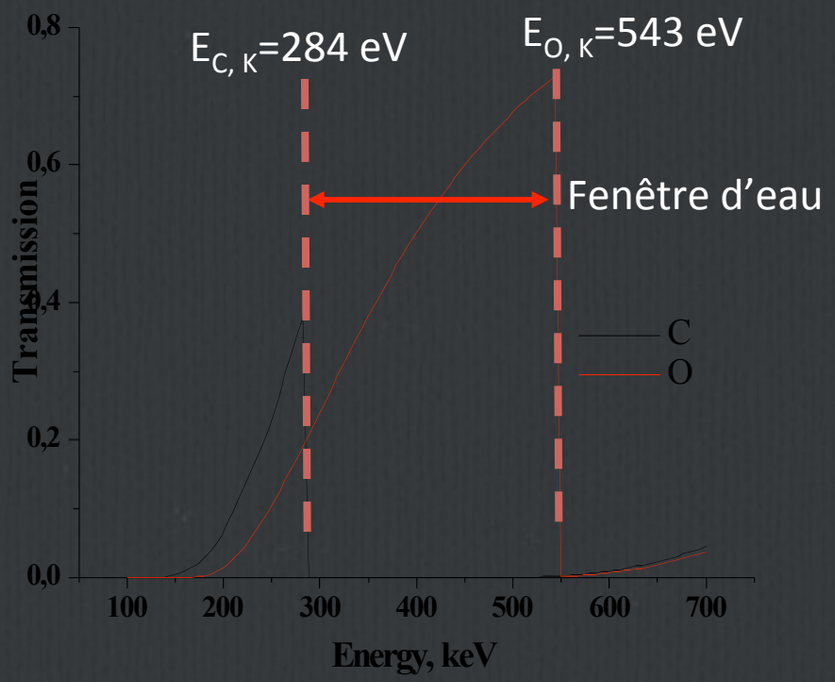
Idéal pour imagerie intact des cellules hydratés d'un épaisseur du quelques μm

imagerie (tomographie) magnifiée:

résolution: 10-30 nm

imagerie cellulaire

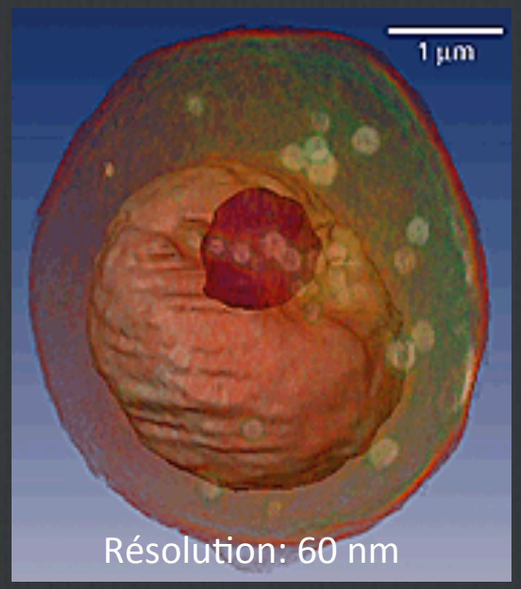




from Andrea SOMOGYI (synchrotron SOLEIL, Nanoscopium)

Absorption X - Water window

Imagerie absorption X – Fenetre de l'eau

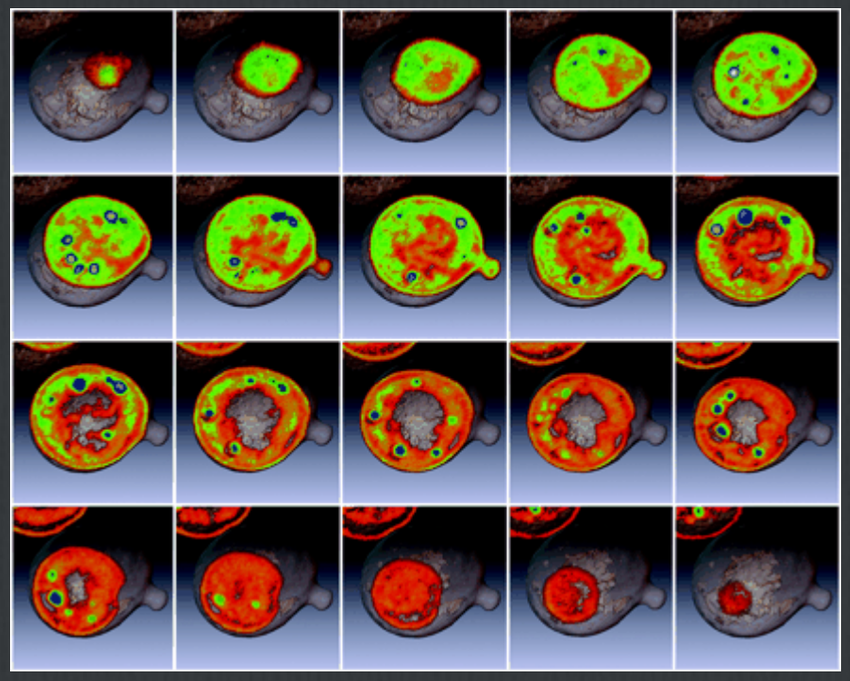


(284 eV <E_0<543 eV)

Organelles internes: différent niveau d'absorption.
- Rouge: nucleus (sphère petite) et vacuole
- Blanc: lipide,
- Orange/vert: structures cytoplasmiques

C.A. Larabell, M.A. Le Gros, *Molecular Biology of the Cell* 15, 957

Reconstruction tomographique du *Saccharomyces cerevisiae* (levure).



cellules hydratés, résolution: ~35 nm

éléments structural spécifique dans le cellule, rés.: ~25 nm

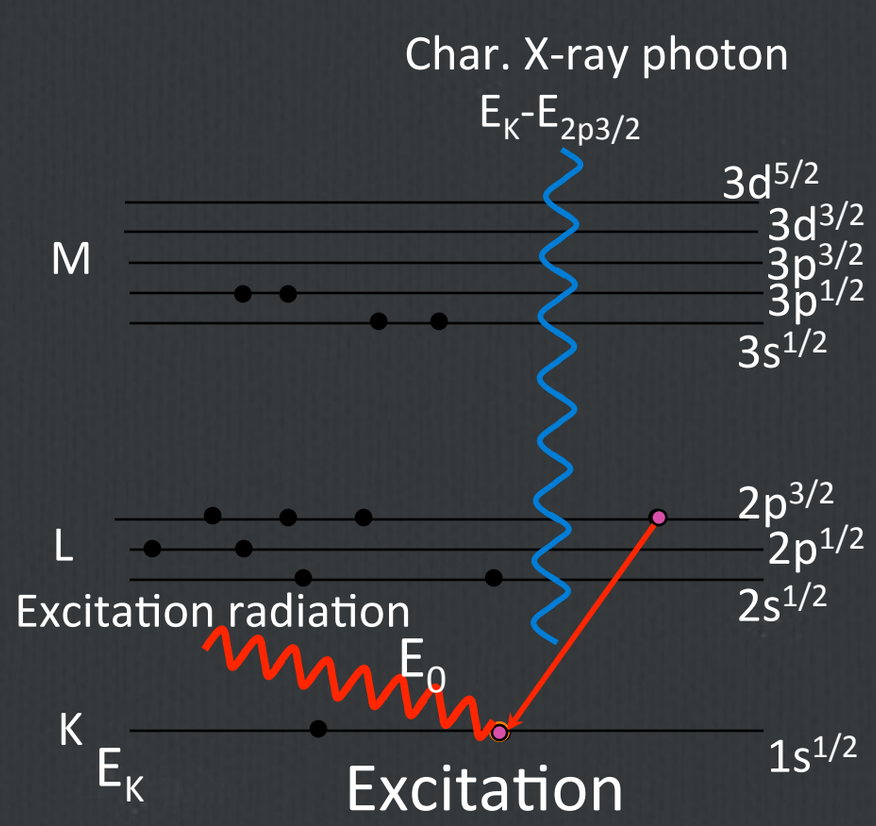
Durée du tomographie: quelques minutes.

from Andrea SOMOGYI (synchrotron SOLEIL, Nanoscopium)

Fluorescence X

Micro spectroscopie de fluorescence X

Excitation des couches électroniques internes (K, L, …) par des rayons X dont l'énergie >énergie d'ionisation du seuil



De-excitation: transitions électroniques

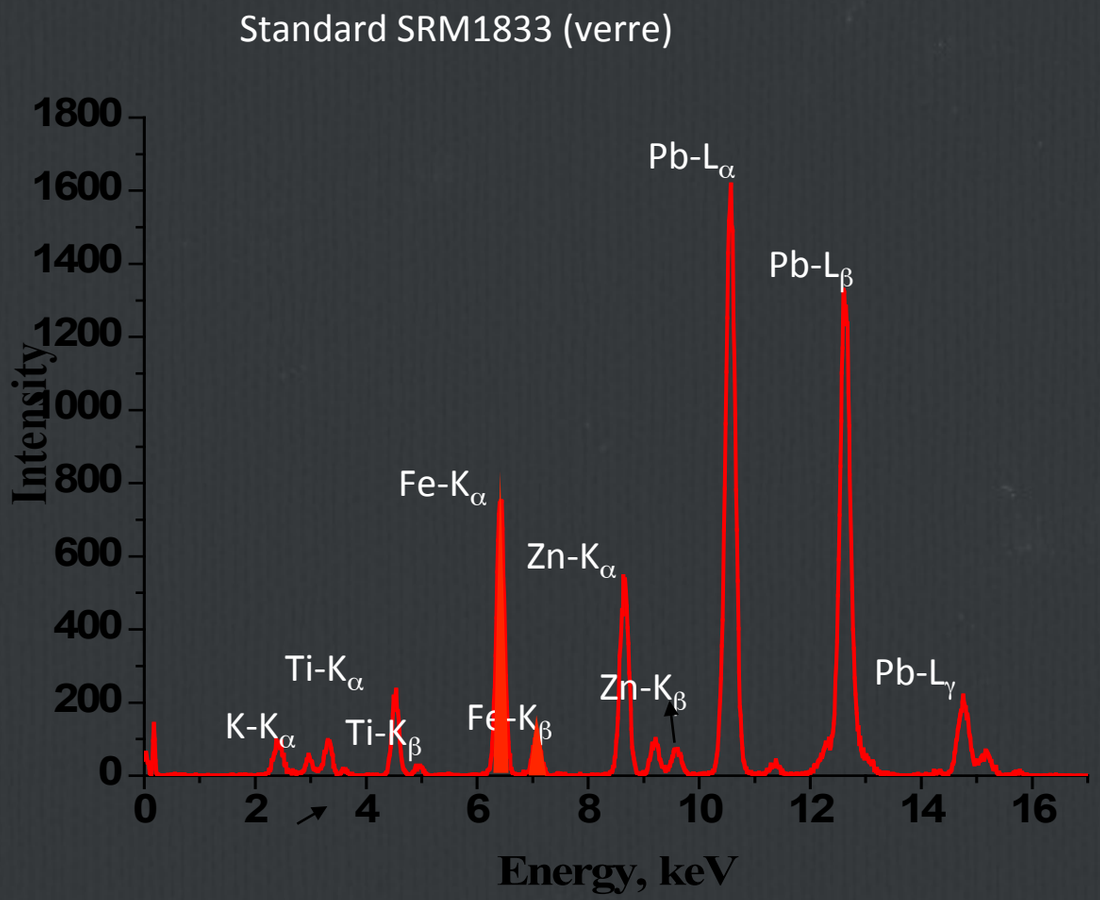
Rayonnement caractéristiques X
énergie (par exemple E_K-E_L)

spectroscopie de fluorescence X

from Andrea SOMOGYI (synchrotron SOLEIL, Nanoscopium)

Fluorescence X

Micro spectroscopie de fluorescence X



Energies des lignes caractéristiques X → analyse qualitative

Intensité d'une ligne caractéristique X → analyse quantitative ~nombre/ concentration des atomes excités

from Andrea SOMOGYI (synchrotron SOLEIL, Nanoscopium)

Fluorescence X

Micro spectroscopie de fluorescence X



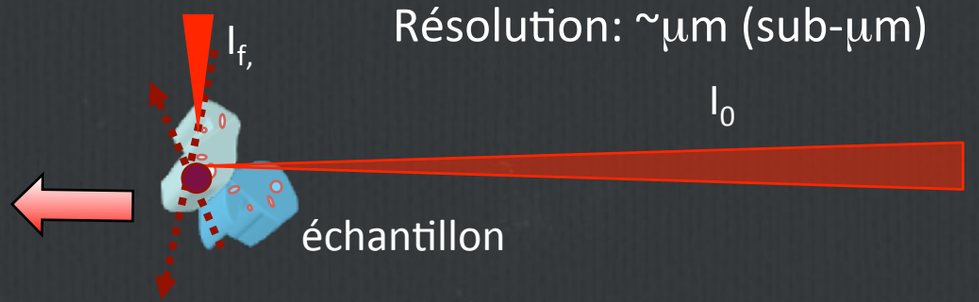
Contrast: fluorescence X, composition élémentaire

détecteur

Faisceau focalisé
Résolution: ~µm (sub-µm)

$I_{f,}$

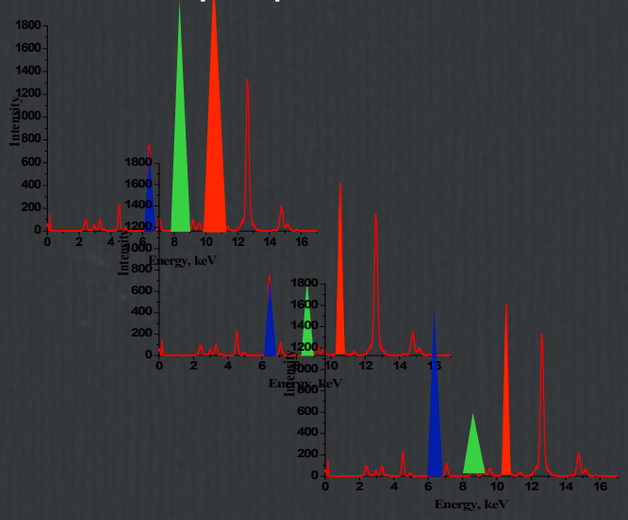
I_0

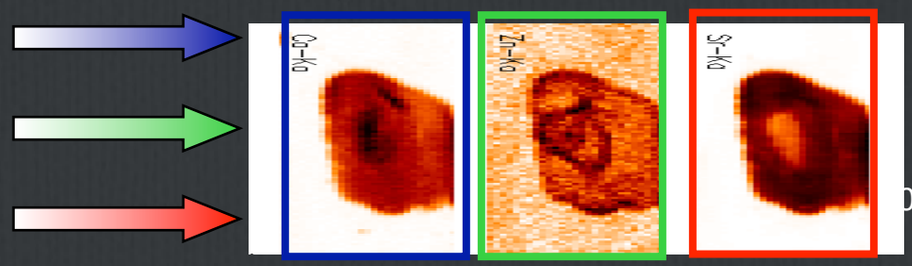


échantillon

Balayage avec l'échantillon dans le faisceau focalisé

spectre de fluorescence X à chaque pixel



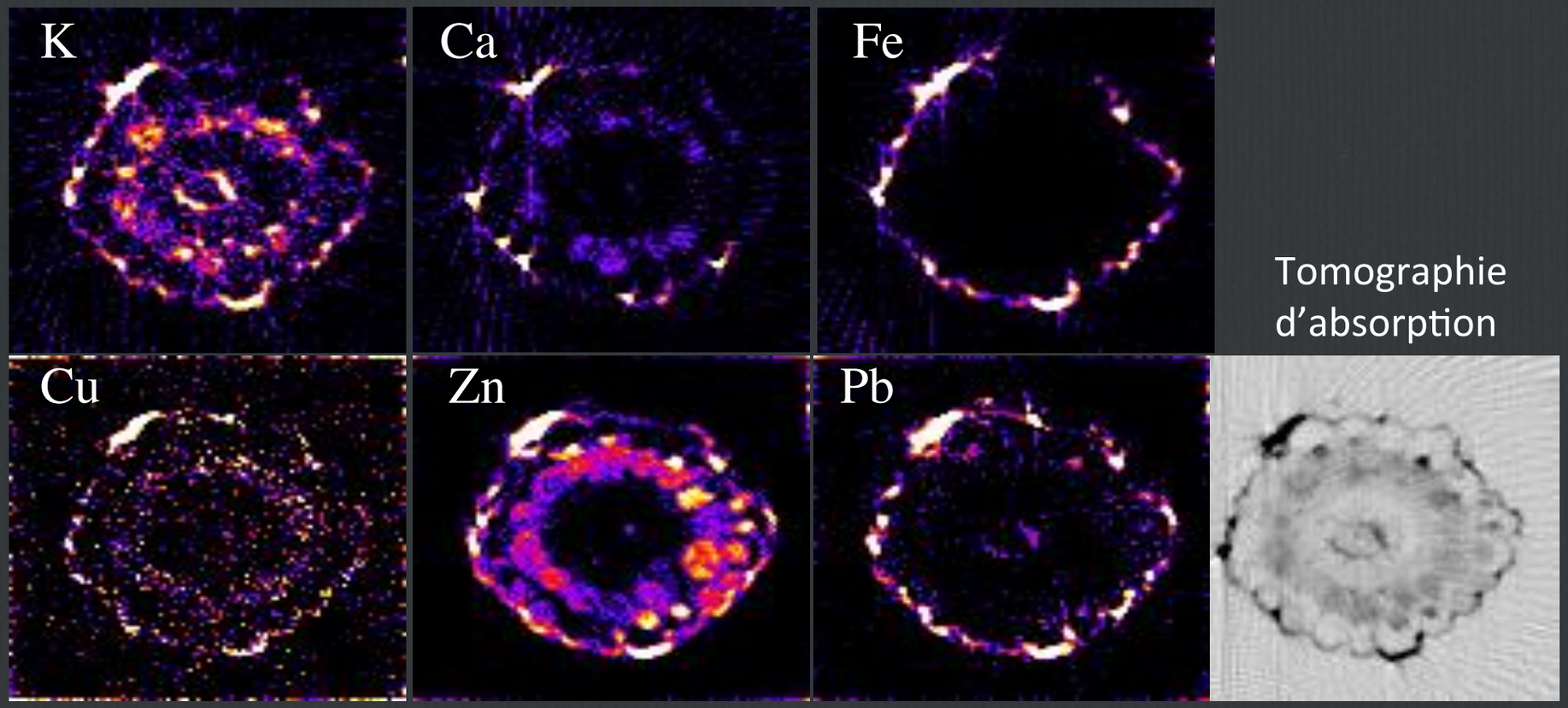


00 µm

from Andrea SOMOGYI (synchrotron SOLEIL, Nanoscopium)

Fluorescence X

Tomographie de fluorescence X: balayage/cartographies sous différentes angles
Reconstruction mathématique



Tomographie d'absorption

Étude du transporte des ions des plants

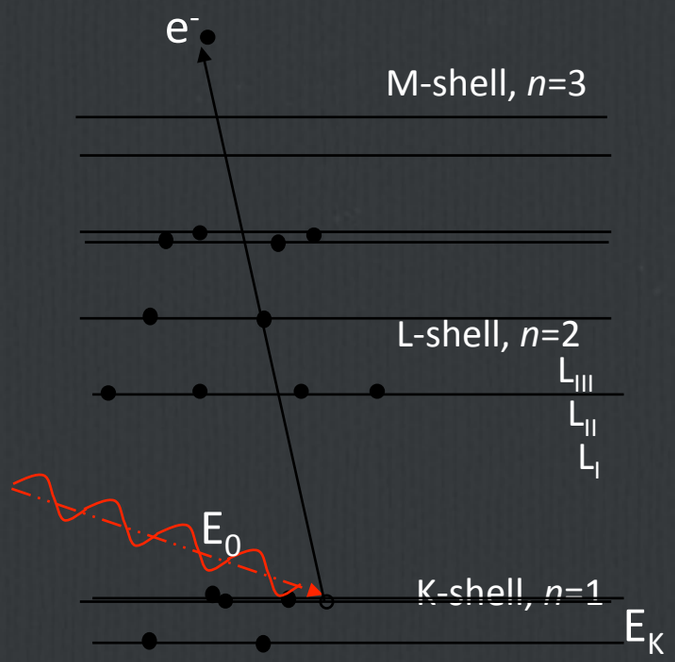
Racine du tomate, Ø < 0.5 mm, résolution ≈ 1 µm

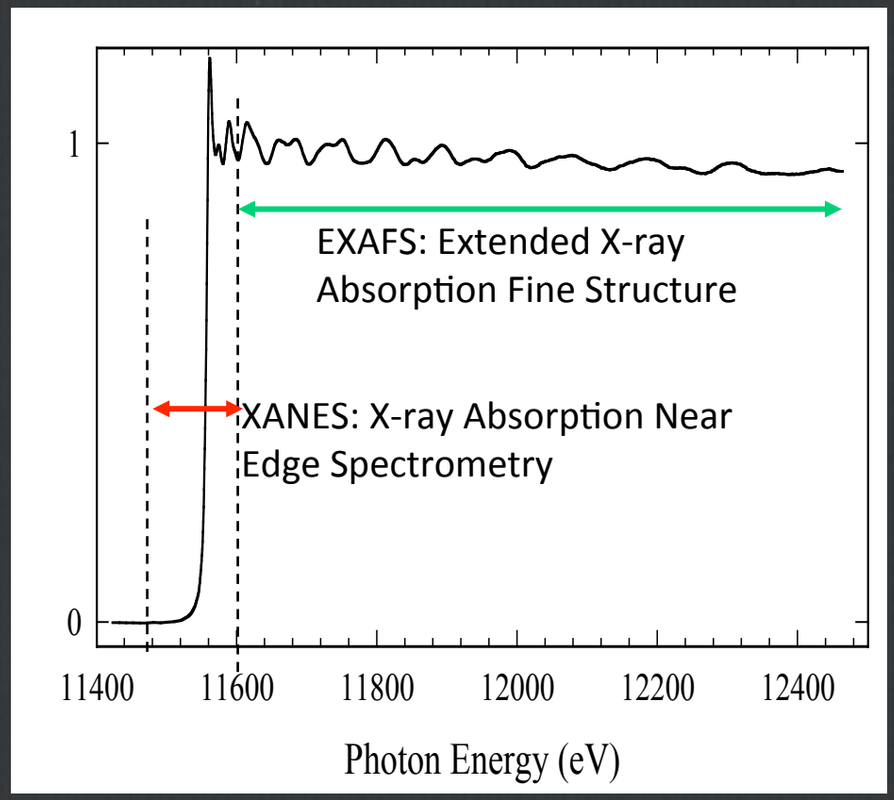
W. Schröder, *et. al.*, RWTH Aachen

from Andrea SOMOGYI (synchrotron SOLEIL, Nanoscopium)

Spectroscopy X

Spectroscopie d'absorption





Changement E_0 au voisinage du seuil d'absorption d'un élément avec une résolution en énergie ~eV

XANES: environnement chimique, état d'oxydation d'un élément mesuré
EXAFS: provides detailed information on the local environment of the target atom; co-ordination numbers and bond lengths.

from Andrea SOMOGYI (synchrotron SOLEIL, Nanoscopium)